

AN ULTRASTRUCTURAL INVESTIGATION  
OF CHOLINERGIC NEUROMODULATORY AXONS  
IN THE BARREL CORTEX

**Master's Thesis**

in partial fulfilment of the requirements  
for the degree “Master of Science”  
in the Neuroscience Program  
at the Georg August University Göttingen,  
Faculty of Biology

submitted by

**Daniela Doda**

born on 25.08.1994 in Albania

in June 2019

<b>First supervisor:</b>	Dr. Graham Knott
<b>Second supervisor:</b>	Prof. Dr. Carl Petersen
<b>First referee:</b>	Prof. Dr. Jochen Staiger
<b>Second referee:</b>	Prof. Dr. Martin Göpfert
<b>Date of submission of the Master's Thesis:</b>	30.06.2019
<b>Date of written examination:</b>	20.08.2018
<b>Dates of oral examinations:</b>	22. & 23.08.2019

# **Abstract**

The neurotransmitter acetylcholine has wide-ranging effects on brain functions, by modulating and shaping neuronal activity, synaptic transmission and plasticity. The main source of cholinergic axons in the cortex is the basal forebrain, whose neurons project widely across the brain. However, despite physiological evidence that suggests a direct effect of acetylcholine on the interneurons that inhibit pyramidal neurons, there is no structural evidence of these specific synaptic contacts. To address this question and characterize the nature of cholinergic contacts onto interneurons, we used a correlative light and electron microscopy technique to target two types of inhibitory cell types: vasoactive intestinal peptide (VIP) and parvalbumin (PV) expressing interneurons, and investigated their interactions with cholinergic axons. We reconstructed and characterized the VIP- and PV-expressing cells, analysing their synaptic inputs and possible connections with cholinergic axons. Results show that dendritic spines are absent from PV+ neurons with only few spines on the VIP+ cell, although both had similar numbers of excitatory inputs on the dendritic shaft. Regarding the cholinergic connectivity with these cell types, axons appear to be closely apposed to the VIP+ and PV+ interneurons, particularly at their somata. However, there is limited evidence of typical synaptic connections with clear features that would allow us to classify these sites as synapses. Nevertheless, the abundance of vesicles and contacts with the membranes could represent regions of possible communication. This finding suggests that the connectivity between the cholinergic neurons and these interneurons in the cerebral cortex may not appear as typical synaptic connections, raising questions about how the connectivity of neuromodulatory axons should be characterized.

# Contents

<b>Abstract</b>	<b>III</b>
<b>1 Introduction</b>	<b>1</b>
1.1 The barrel cortex and GABAergic inhibitory interneurons . . . . .	1
1.1.1 Barrel cortex structure and function . . . . .	1
1.1.2 Barrel cortex cell composition . . . . .	1
1.2 The VIP-expressing interneurons . . . . .	3
1.3 The PV-expressing interneurons . . . . .	3
1.4 Acetylcholine in the cortex . . . . .	5
1.5 3D electron microscopy . . . . .	7
1.6 Aim of the project . . . . .	7
<b>2 Methods</b>	<b>9</b>
2.1 Animals . . . . .	9
2.2 Fluorescence and light microscopy . . . . .	9
2.3 Tissue and block preparation for electron microscopy . . . . .	10
2.3.1 Tissue embedding . . . . .	10
2.3.2 Alignment and block preparation . . . . .	10
2.4 Serial Block-Face EM imaging . . . . .	12
2.5 EM image processing, segmentation and 3D model generation . . . . .	13
2.6 Blender and 3D model processing . . . . .	13
2.7 Statistical analysis . . . . .	13
<b>3 Results</b>	<b>14</b>
3.1 Transgenic animals . . . . .	14
3.2 Morphological description of the VIP-expressing interneuron cell body and nucleus . . . . .	14
3.3 Morphological analysis of VIP-expressing interneurons' dendrites . . . . .	16
3.4 Morphological description of the PV-expressing interneuron cell body . . . . .	18

3.5	Morphological analysis PV-expressing interneuron dendrites . . . . .	20
3.6	Morphological analysis of ChAT-expressing axons . . . . .	21
3.7	ChAT-expressing axons and their interaction with GABAergic interneurons . . . . .	24
3.7.1	VIP+ interneurons and ChAT+ axons interaction . . . . .	24
3.7.2	PV+ interneurons and ChAT axons interaction . . . . .	24
3.8	VIP+ and PV+ axons characterization . . . . .	24
3.9	Cilium characterization . . . . .	27
<b>4</b>	<b>Discussion</b>	<b>30</b>
4.1	Small sample size limits significance . . . . .	30
4.2	VIP+ and PV+ soma and nuclei are irregularly shaped . . . . .	30
4.3	VIP+ and PV+ dendrites receive excitatory and inhibitory input . . . . .	31
4.4	Comparing synapse sizes of proximal and distal VIP+ and PV+ dendrites	32
4.5	Cholinergic axons form synapse-resembling connections . . . . .	32
4.6	ChAT+ axons contact VIP+, but not PV+ interneurons . . . . .	34
4.7	ECS shrinkage might influence neuronal contact morphology . . . . .	35
4.8	Project outlook . . . . .	36
4.9	Conclusion . . . . .	36
<b>Acknowledgements</b>		<b>44</b>
<b>Declaration of independent work</b>		<b>45</b>

# 1 Introduction

## 1.1 The barrel cortex and GABAergic inhibitory interneurons

### 1.1.1 Barrel cortex structure and function

The neocortex is a six-layered structure in the brain responsible for the execution of higher-order brain functions, such as cognition, sensory perception and sophisticated motor control. Deciphering how information is coded and processed in the neocortex is one of the greatest challenges in neuroscience (Lui et al., 2011; Lodato et al., 2016). The rodent primary somatosensory cortex (S1) or barrel cortex is one of the main model systems for cortical circuitry. Somatosensory information from the vibrissae reach the barrels, dense patch-like structures in layer IV. These barrels have a somatotopic organization, where each whisker is represented by its own barrel column (Feldmeyer et al., 2013; Petersen and Crochet, 2013). Its accessibility, distinct anatomy and comparably easy manipulation make the barrel cortex a well studied system for the complex connectivity and functionality of neocortical networks. When investigating basic microcircuits, working in the barrel cortex offers the benefit of being able to have recourse to decades of research on its constitution and circuitry, making it possible to isolate fine aspects of a complex neuronal system. Afterwards, findings of basic research on the barrel cortex can be generalized to other, less understood cortical regions.

### 1.1.2 Barrel cortex cell composition

The rodent barrel cortex is constituted of excitatory and inhibitory neurons. In each barrel column 80% of the neurons are excitatory while 20% is inhibitory (Markram et al., 2004). The excitatory neurons are homogeneous principal cells (PCs) that use glutamate as a neurotransmitter. The inhibitory components, on the contrary, are extremely diverse regarding morphological, organizational, electrophysiological and ge-

netic aspects. Cortical inhibition is mainly mediated by the GABAergic interneurons. Different types of GABAergic interneurons strongly govern the activity of cortical circuits towards meaningful behavior by feed-forward and feedback inhibition as well as disinhibition (fig. 2, Staiger et al. (2015)). A first classification is made according to non-overlapping markers such as parvalbumin (PV, a  $\text{Ca}^{2+}$ -binding protein, ~40%), somatostatin (SST, ~30%) and the ionotropic serotonin receptor 5HT3a (5HT3aR, ~30%). Each group has a different embryological origin and contains further subdivisions (Staiger et al., 2015; Tremblay et al., 2017; Rudy et al., 2011).

These inhibitory interneurons are thought to contribute to a variety of cortical functions such as gamma oscillatory activity, learning and plasticity (Kuki et al., 2015; Fu et al., 2015; Li et al., 2015). Malfunctioning of inhibitory neurons are also implicated in a variety of pathological conditions like epilepsy (Cobos et al., 2005), schizophrenia (Rogasch et al., 2014) and bipolar disorder (Levinson et al., 2007). Therefore, gaining an understanding of cortical connections in the neocortex through the characterization of the different cell type populations and how they are coded and modulated into circuits remains a major focus of research.

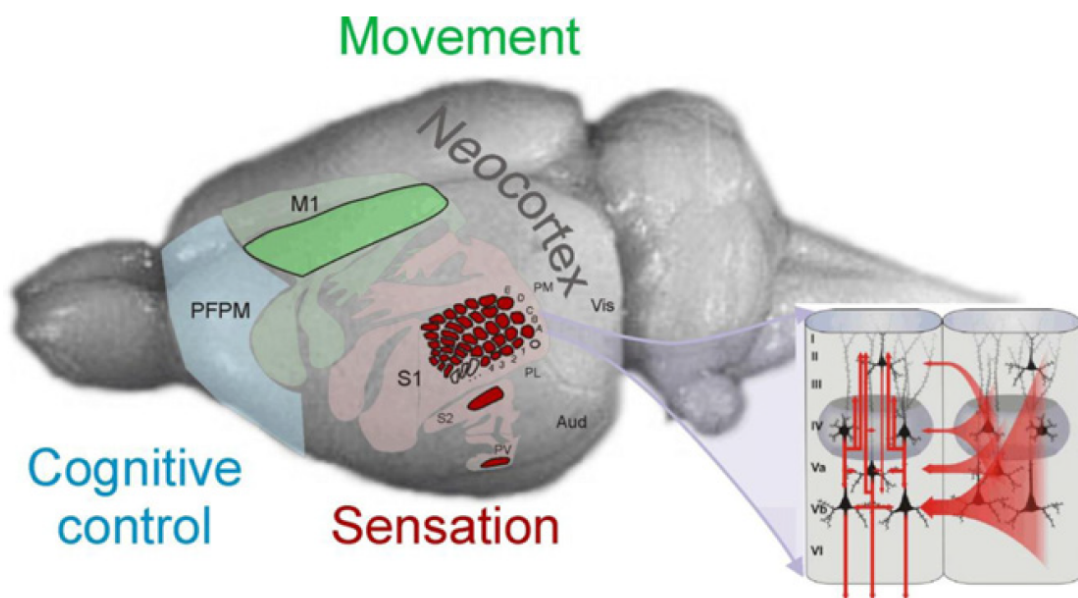


**Figure 1: Organization of the barrel cortex.** The barrels are dense patches in layer IV of the rodent primary somatosensory cortex. Each barrel receives input from one whisker in a somatotopic organization. Aside from the dense connectivity in each barrel, cross-talk between barrels as well as modulation from other brain areas occurs. From Feldmeyer et al. (2013).

## **1.2 The VIP-expressing interneurons**

Neurons expressing VIP belong to the ionotropic serotonin receptor (5HT3aR)-positive cells that produce  $\gamma$ -aminobutyric acid (GABA). Cortical VIP neurons are key elements in neurovascular coupling (Cauli et al., 2004) and in the regulation of neuronal energy metabolism (Magistretti and Pellerin, 1999). In terms of cortical circuitry, it has been repeatedly reported that VIP neurons preferentially target several other types of inhibitory interneurons (Staiger et al., 2004; David et al., 2007; Pfeffer et al., 2013), thus mediating disinhibition by releasing excitatory principal neurons from inhibition (fig. 4, Wang and Yang (2018)). The resulting disinhibitory circuit motif involving the VIP-to-SST connectivity has now been functionally characterized in the visual (Fu et al., 2014; Zhang et al., 2014), the auditory (Pi et al., 2013), and the S1 barrel cortex (Lee et al., 2013; Wang and Yang, 2018).

The VIP neurons in the barrel cortex are not homogenously distributed across layers with densities ranging from  $44.6 \pm 40.5$  cells/mm<sup>3</sup> cortex in layer I to  $1366.6 \pm 285.8$  cells/mm<sup>3</sup> in layer II/III. This compartment presents the highest number of VIP-positive cells, accommodating 58.7% of the total VIP cell number in the barrel cortex (Proenneke et al., 2015).

The morphological organization of VIP+ interneurons depends on the layer they are located in. The soma is generally elliptic with a larger vertical than horizontal diameter. VIP+ cells can be categorized in two groups by their dendritic structure: bipolar and bitufted cells. The former have two big dendrites with few branches that emerge on opposite sides of the cell body. The latter have more irregular features and usually more than 2 dendrites (Feldmeyer et al. (2013), see fig. 9)

## **1.3 The PV-expressing interneurons**

The PV+ interneurons express the calcium-binding protein parvalbumin (PV), and constitute with 40% the largest group of GABAergic interneurons (Celio, 1986). These cells have a high density in layer IV and present two main subclasses: the basket and axon-axonic (or chandelier) cells (fig. 2, Markram et al. (2004)). PV+ interneurons have multiple dendrites which are highly ramified and distributed across layers which allows these interneurons to receive input from different afferent pathways, such as feedforward and feedback pathways (Hu et al., 2014). Electrophysiologically, these cells are characterized by a fast spiking activity due to the expression of AMPA-like

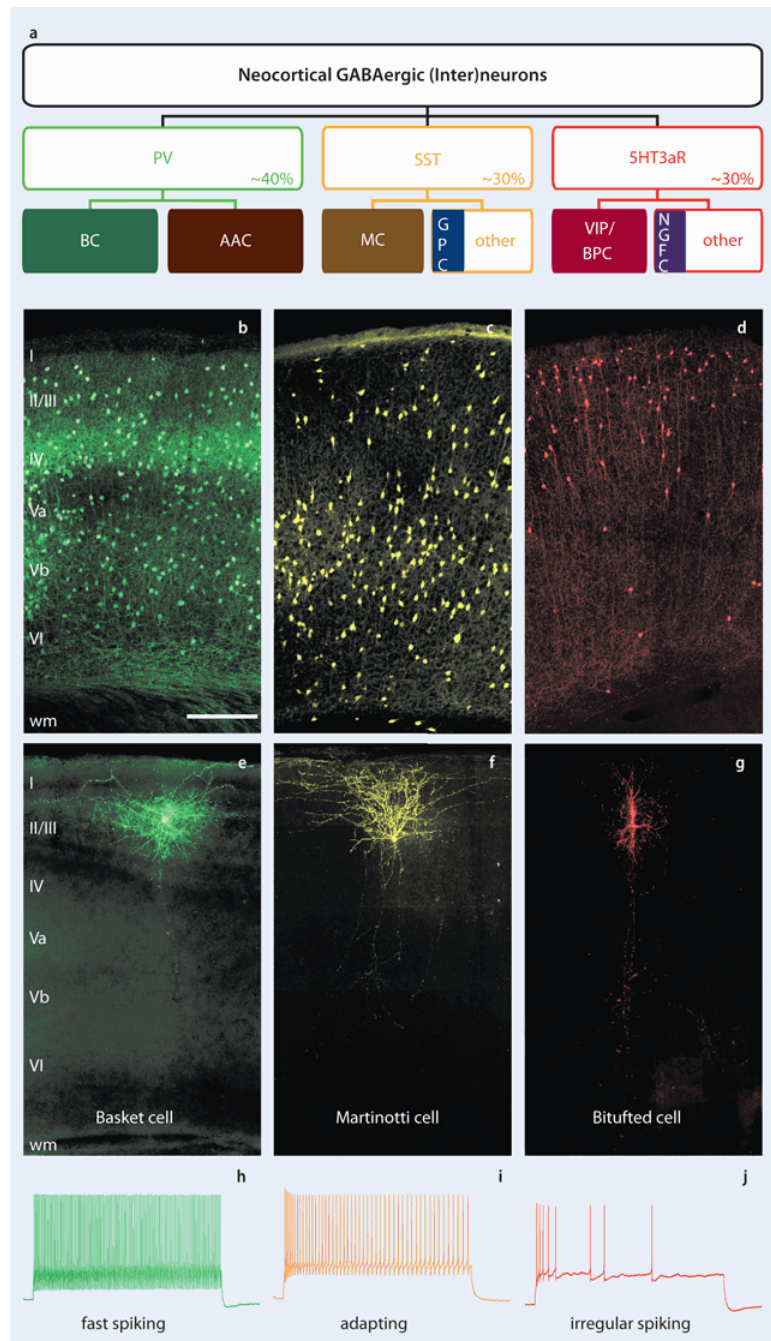


**Figure 2: Scheme showing the different types of GABAergic interneurons. (b-d)**  
 Overview of the barrel cortex in tissues expressing markers for PV (green), SST (yellow) and VIP (red). (e-g) Reconstructions of a PV-expressing, fast-spiking basket cell, a somatostatin-expressing, adapting Martinotti cell and a VIP-expressing, irregular-spiking bitufted cell. (h-j) Representation of action potential firing patterns of aforementioned cell types. From Staiger et al. (2015).

glutamate receptors with high  $\text{Ca}^{2+}$  permeability and fast gating (Kawaguchi et al., 1987; Geiger et al., 1995). The PV+ cells modulate the perisomatic activity of the PCs by controlling their spiking output (Tremblay et al., 2017; Wang et al., 2017). As mentioned in chapter 1.2, the cortical interneurons form an disinhibitory circuit where the PV+ cells play an important role innervating the PC's cell body.

## 1.4 Acetylcholine in the cortex

Recently, acetylcholine (ACh), the main neurotransmitter at neuromuscular junctions and in the autonomous nervous system, has been found to modulate and shape the neuronal activity, the synaptic transmission and the synaptic plasticity of the central nervous system (CNS; Alitto and Dan (2013); Fu et al. (2014); Picciotto et al. (2012)). ACh is mainly produced by cholinergic neurons of the basal forebrain (BF) that project to different areas of the cortex including the barrel cortex (fig. 3; Thiele (2013)). These cholinergic projections enhance or inhibit a circuit where the VIP+ cells inhibit the SST+ cells, which in turn disinhibits the excitatory PCs (Pfeffer et al., 2013). ACh acts on two different receptors: muscarinic (mAChR) and nicotinic (nAChR) receptors. When ACh acts on the mAChR, it induces activity of PCs and PV+ interneurons, whereas binding to nACh activates VIP+ cells (Alitto and Dan, 2013).

This divergent effect of ACh is correlated to the resulting cortical neuronal state: synchronization (mACh activation, quiet wakefulness) and desynchronization (nACh activation, active behavior such as whiskering; Crochet and C H Petersen (2006); Eggermann et al. (2014)).

Recently, a study of the disinhibitory circuit in the S1 showed that only a specific subtype of SST+ interneurons is inhibited during whisking behavior. This SST+ suppression was mediated by VIP+ cells (Munoz et al., 2017). A critical finding for our project is the ACh-induced enhancement of VIP+ activity in the primary visual cortex (V1, Fu et al. (2014); Pinto et al. (2013)). By using in-vivo calcium imaging, it was

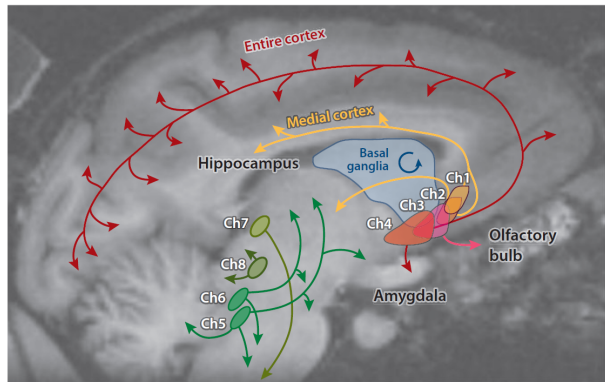


**Figure 3: Acetylcholine distribution in the cortex.** Acetylcholine is produced by a few brainstem and basal forebrain nuclei. From there, projecting axons distribute ACh throughout the CNS. From Thiele (2013).

correlated to the resulting cortical neuronal state: synchronization (mACh activation, quiet wakefulness) and desynchronization (nACh activation, active behavior such as whiskering; Crochet and C H Petersen (2006); Eggermann et al. (2014)).

Recently, a study of the disinhibitory circuit in the S1 showed that only a specific subtype of SST+ interneurons is inhibited during whisking behavior. This SST+ suppression was mediated by VIP+ cells (Munoz et al., 2017). A critical finding for our project is the ACh-induced enhancement of VIP+ activity in the primary visual cortex (V1, Fu et al. (2014); Pinto et al. (2013)). By using in-vivo calcium imaging, it was

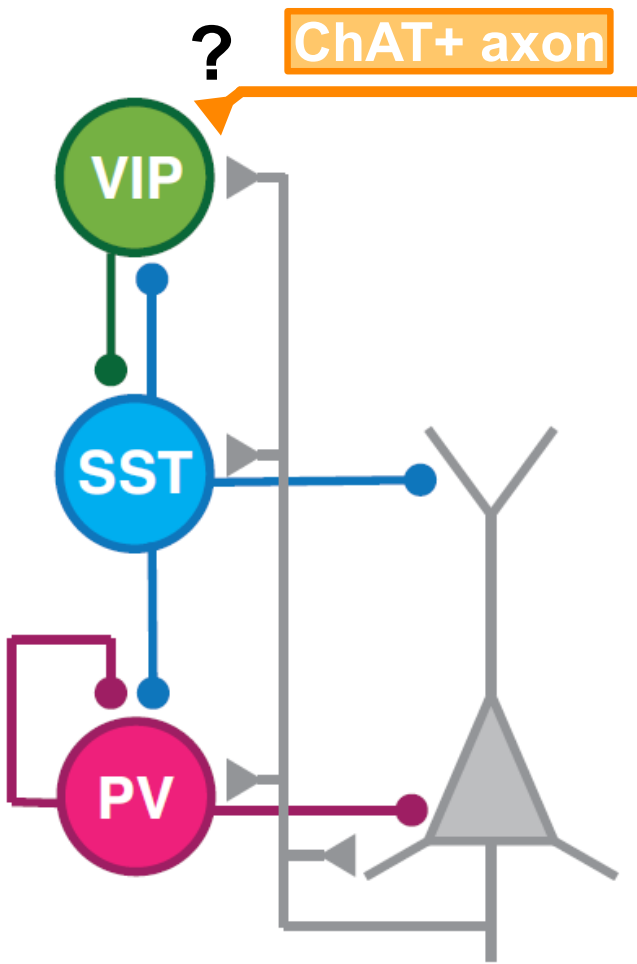


**Figure 4: Proposed cortical disinhibitory microcircuit.** In this model, SST+ neurons inhibit distal dendrites and PV+ cells target the soma of excitatory pyramidal cells (grey), suppressing excitatory output of the microcircuit. VIP+ interneurons target SST+ cells. Thus, VIP+ activity inhibits SST+ neurons, lifting their suppression on principal cells and increasing the excitation of the circuit via disinhibition. The precise connectivity, especially of PV+ interneurons, is still under debate. Other studies have shown that ACh released from ChAT+ axons, originating in basal forebrain nuclei, can influence the activity of VIP+ cells, thus possibly modulating the entire circuit (Alitto and Dan, 2013). However, the nature of communication between ChAT+ axons and VIP+ neurons is still unclear. Adapted from Wang and Yang (2018).

discovered that during locomotion VIP+ interneurons were active, independently of visual stimuli (Fu et al., 2014). At the same time, SST+ cells were inactive. Additionally, optogenetic stimulation of the BF cholinergic neurons enhanced visual perception and cortical activity in V1 (Pinto et al., 2013). These findings support the circuit proposed by Pfeffer et al. (2013) where VIP+ interneurons enhance the nearby PCs by inhibiting SST+ neurons (fig. 4).

Although the effect of ACh in the cortex has been shown, no study has reported cholinergic synapses in the barrel cortex. Instead, ACh is thought to be released via volume transmission, release ACh untargeted into the extracellular matrix (ECM). However, ACh has been shown to act faster on target cells than would be expected for volume transmission (Fu et al., 2014). The hypothesis of this project is that there are cholinergic synapses on the L2/3 VIP+ neurons in the barrel cortex. To demonstrate

this, we are going to use correlated light and electron microscopy (CLEM).

## **1.5 3D electron microscopy**

Since the 1930s, electron microscopy (EM) has played an important role in describing the ultrastructure of biological samples (Knott and Genoud, 2013). Therefore, various techniques have been developed to overcome some of its limitations such as structure-obscuring immunolabeling, narrow fields of view, volume imaging and fixation-induced tissue shrinkage. In this project, we avoid antibody-labelling of structures by using transgenic mice that express fluorescent proteins in the cells of interest. Moreover, we are using a correlative light and electron microscopy (CLEM) method developed by Maclachlan et al. (2018). Briefly, characteristic tissue landmarks such as cell bodies or capillaries are identified via light microscopy, which are then used to locate the same region under the electron microscope. In order to create large-scale reconstructions of neuronal structures and to obtain 3D models of the reconstructed cells, we use a serial block face scanning EM (SBEM) equipped with the 3View system (see ch. 2.4). This is a automated volumetric EM technique where thin sections are constantly removed from the resin block surface, yielding a nearly complete reconstruction of the complete sample block. Additionally, several tiles of the same surface can be imaged and later aligned to increase the originally narrow field of view. These techniques provide a high-resolution volumetric dataset the sample free from immunostaining.

## **1.6 Aim of the project**

Acetylcholine has been shown to affect VIP+ interneurons with a specificity and temporal resolution presumably too high for pure volume transmission, although synapses of ChAT+ axons onto cortical GABAergic interneurons have not been shown yet. We hypothesize that the cholinergic axons projecting from the BF are making synapse-like connections onto the GABAergic interneurons of the barrel cortex. We will focus on L2/3 VIP+ and PV+ cells. To assess our hypothesis, we will use two transgenic mouse lines where EYFP and tdTomato mark the ChAT+ axons and VIP+ or PV+ cells respectively. These structures are imaged simultaneously, allowing for interaction studies. To understand these connections, we will use correlated light and electron microscopy (CLEM) where regions of interest imaged in fluorescence microscope are assessed at a ultrastructural level via electron microscopy and later reconstructed to

---

*INTRODUCTION*

3D models. Besides characterizing these reconstructed neuronal structures, this technique will allow us to investigate the connectivity of cholinergic axons onto GABAergic interneurons at nanoscale resolution.

## 2 Methods

### 2.1 Animals

All experiments were performed according to the guidelines of the Swiss Federal Act on Animal Protection and Swiss Animal Protection Ordinance with licences granted to Professor Carl Petersen. For this study we employed VIPcre-tdTomato/ChAT-ChR2-EYFP and PVcre-tdTomato/ChAT-ChR2-EYFP transgenic mouse lines. The mice were anaesthetised with isoflurane and chemically fixed via transcardial perfusion of 10 ml of isotonic phosphate buffer saline (PBS), followed by 200 ml of 1 % glutaraldehyde and 2% paraformaldehyde (PFA) in phosphate buffer (PBS, 0.1 M, pH 7.4).

Once perfused, animals were left at room temperature (RT) for 2 h. The brains were then removed from the skull and embedded in 5 % standard agarose (Eurobio) dissolved in PBS. 80  $\mu$ m thick coronal slices were cut through the region of the primary somatosensory cortex (S1) using a vibratome chamber (Leica VT1200 S).

### 2.2 Fluorescence and light microscopy

To visualize tdTomato and EYFP expression in the transgenic mice, an inverted confocal microscope (Zeiss LSM 700 Invert) was used and Z-stacks with 2  $\mu$ m interplanar distance were acquired at different magnifications (40X, 20X, 10X) to later locate target cells. Emissions of EYFP and tdTomato were recorded at 488 and 546 nm wavelength respectively. VIP/PV expressing cells in layer II/III of S1 with multiple adjacent ChAT+ axons were targeted. Additionally, images were collected using transmitted light to detect slice-specific morphological landmarks such as cell bodies and blood vessels. To maintain high tissue quality and good ultrastructural preservation, the brain slices were kept in PBS throughout the imaging process. To ensure that the slices did not dry out, custom-made chambers consisting of a glass microscope slide, parafilm and a cover glass was used (fig. 5).

Afterwards, the slices were brought under a dissecting light microscope (Leica M205 C) containing a camera (Leica MC170 HD). The brain slices were divided along the midline and low magnification images of the entire hemisphere previously imaged under the confocal microscope were collected.

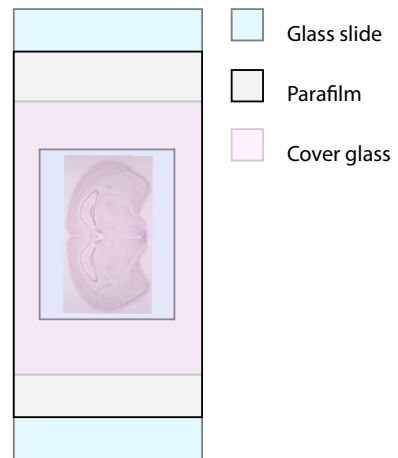


**Figure 5:** Schematic illustration of the imaging chamber

## 2.3 Tissue and block preparation for electron microscopy

### 2.3.1 Tissue embedding

Following the fluorescence and light microscopy, slices were stained and embedded using methods described in Knott et al. (2011). Briefly, the slices were washed in cacodylate buffer (0.1 M, pH 7.4, 3 × 5 min each), post fixed in 2% osmium tetroxide (Electron Microscopy Sciences, 19110) and 1.5% potassium ferrocyanide (Sigma 14459-95-1) in cacodylate buffer (0.1 M, pH 7.4, 40 min). They were then stained with 2% osmium tetroxide in cacodylate buffer (0.1 M, pH 7.4) for 40 min, and then in 1% uranyl acetate at 4°C overnight. Then the sections were stained in lead aspartate for 2 h, dehydrated in a graded alcohol series for 5 min each, and finally sections were left in Durcupan resin (Electron Microscopy Sciences, 13600) and ethanol solution (1:1) for 30 min. Between each step, the sections were washed in distilled water at RT. After infiltrating overnight, the sections were placed between two glass slides coated in a mold separating agent (Glorex Inspirations, Switzerland; 62407445) and placed in the oven at 65°C for 24 h.

### 2.3.2 Alignment and block preparation

After Durcupan resin polymerization, the glass slides were separated and the slices stabilized in a thin resin layer. Because sections were impregnated with heavy metals and completely opaque to transmitted light, only their outline could be aligned with the LM images taken before undergoing heavy metal staining (fig. 6A-C). Overlaying the images acquired before and after heavy metal staining allowed for the location of

the regions of interest. These alignments were done in Adobe Photoshop, matching the section edges to identify the region of interest (ROI). The ROI was removed using a razor blade and glued to an aluminium scanning electron microscope (SEM) pin (Micro to Nano place, 10-006002-50) with an electrically conductive epoxy resin (Ted Pella Inc, Redding, CA, USA, 16043). The pin with the sample attached was left overnight at 65°C to polymerize. The following day the block was trimmed using a glass knife mounted in an ultramicrotome (Leica EM UCT). During the trimming, images of the block were imaged frequently to monitor the exact position of the ROI (fig. 6E).

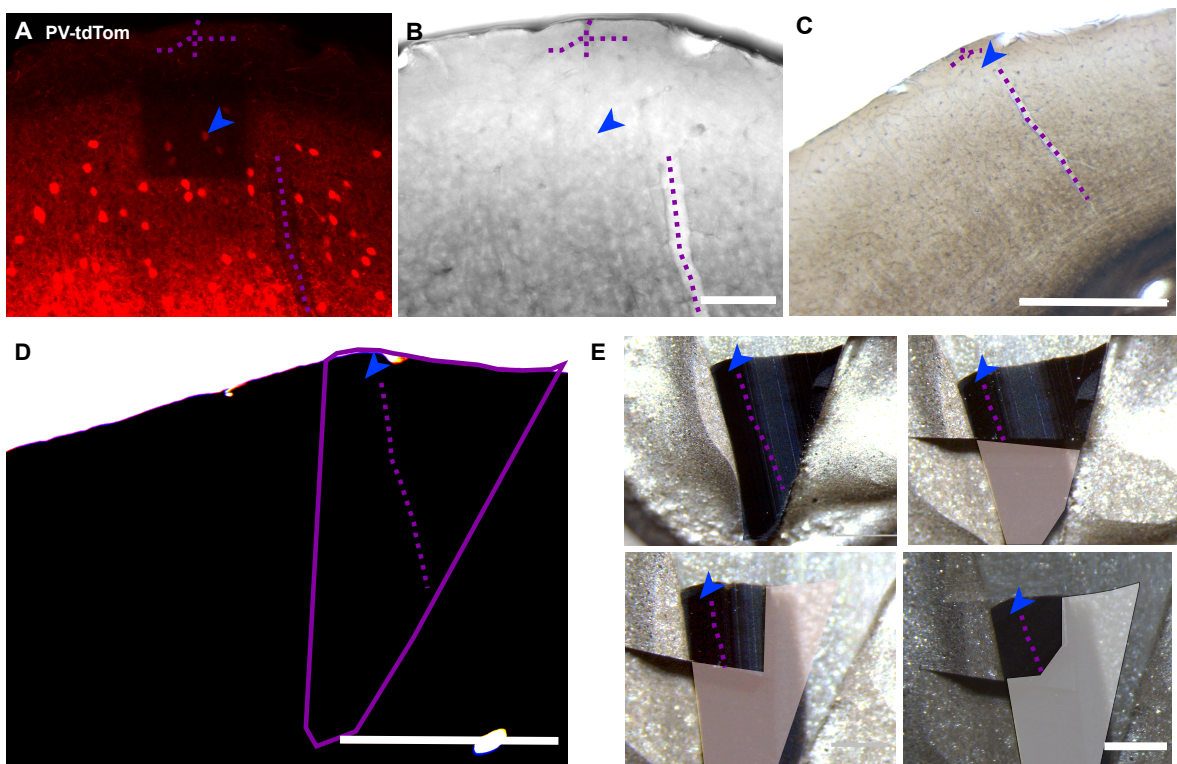


**Figure 6: Illustration of the block preparation process.** (A and B) Low magnification (10X) representative images of the tdTomato channel and transmitted light. (C and D) LM images of the same region shown in A and B before and after heavy metal staining. (E) LM images showing different trimming process steps. Blue arrow indicates location of reconstructed cell in the ROI. Purple dashed lines show capillaries used as landmarks. Scale bars = 500 µm.

## 2.4 Serial Block-Face EM imaging

Before loading the sample into the SEM microscope (Merlin, Zeiss NTS) fitted with the 3View cutting system (Gatan, Inc., Pleasanton, CA, USA), a 40 nm gold coating was applied to the block surface. This is necessary to improve the conduction of the surface and limit imaging artifacts caused by the build up of electrical charge. The first cuts were conducted with an open microscope chamber to remove the gold coating. Then the chamber was closed and pumped to a high vacuum. Next, a low resolution scanning of the block face was acquired to reveal the position of blood vessels seen in the LM images (fig. 7B, D). To determine the exact ROI, a final overlay of the EM block face was made with the LM images. At this point we proceeded to cut away sections from the surface of the block, constantly monitoring the surface in relation to the height of the ROI. For imaging following settings were used: EHT = 1.7 kV; current beam = 300 pA; knife cutting speed = 0.3 mm/sec; backscatter detector = on; image size = 6000 x 6000 pixels, resolution = 6.5 nm x and y; slice thickness = 50 nm. Several tiles per slice were acquired for a larger field of view.

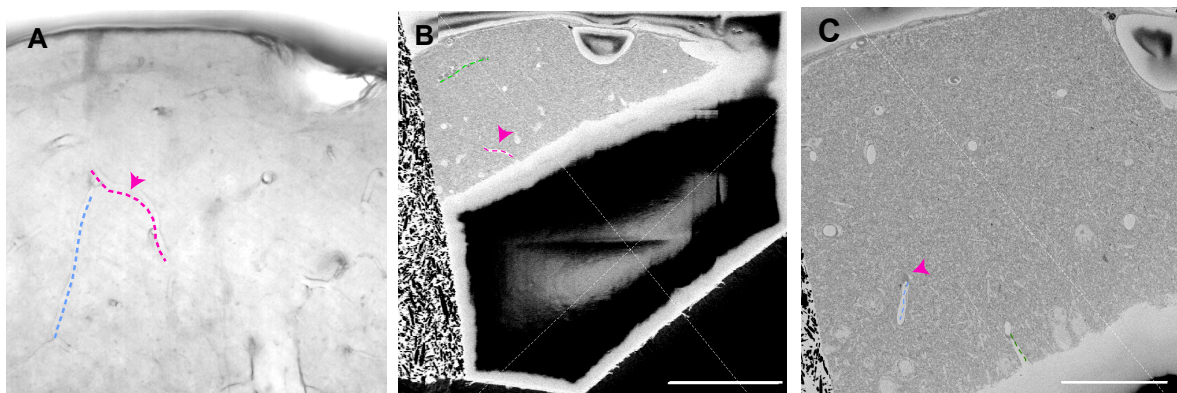


**Figure 7: Low resolution block face images.** (A) Transmitted light image showing the pattern of blood vessels on the slice. (B) Block face overview at low resolution showing blood vessels and cell bodies. (C) Low resolution EM image of the block face at a lower z-depth. Dashed lines indicate landmark capillaries, arrows show target cell. Scale bar = 500  $\mu$ m.

## **2.5 EM image processing, segmentation and 3D model generation**

The raw stacks of images collected from the microscope were first aligned in Fiji with the TrackEM 2 plugin. The alignment function exported the stack in a xml file which was opened in TrackEM 2 to perform the segmentation process. The same plugin was used to trace and segment the features of interest, and create the 3D models. Once the tracing was completed, 3D models were exported as obj files and further processed and analyzed in Blender ([www.blender.org](http://www.blender.org)).

## **2.6 Blender and 3D model processing**

Each segmented object was drawn as an area list in TrackEM 2 and imported into the Blender workspace running the Neuromorph extension (Jorstad et al. 2018). This implementation enable various measurement to be made, such as of surfaces area,, lengths and volumes. Here it was used to measure synapse area, cell body volumes and various lengths.

## **2.7 Statistical analysis**

Neuromorph measurements were processed and analysed with Microsoft Excel 2019. Statistical analysis and plotting was performed with Prism7 (GraphPad Software, San Diego, USA). Synaptic input was analyzed with the excitatory input ratio which was calculated with the following formula:  $\frac{N_{ex}/l_d}{N_{inh}/l_d}$ , with  $N_{ex}$  and  $N_{inh}$  being the numbers of excitatory and inhibitory synapses, which are both normalized against the total length of reconstructed dendrites  $l_d$ . Results are reported as mean +/- SEM. Statistical tests are described in the respective figure legends. Statistically significant P-values are displayed in graphs as: \*  $P<0.05$ , \*\*  $P<0.01$ , \*\*\*  $P<0.001$ .

# **3 Results**

## **3.1 Transgenic animals**

This project examines the interactions between GABAergic interneurons and acetyl cholinergic axons in the barrel cortex. To identify cell types, I used transgenic mice that express fluorescent proteins in my structures of interest. Cholinergic axons are labelled with choline-acetyltransferase-driven EYFP expression in the ChAT-ChR2-EYFP mouse line (fig. 8A; Zhao et al. (2011)). Interneurons are labelled with tdTomato expression driven by VIP and PV reporters respectively (fig. 8B, C; Taniguchi (2012); Arber et al. (2015)). Through crossing of ChAT mice with either VIP (fig. 8D) or PV mice (fig. 8E), simultaneous labelling of both structures allow investigating their interaction. Unfortunately, tdTomato has a wide excitation spectrum which overlaps with EYFP, creating bleed-through in the EYFP (green) channel (fig. 8D, E). The narrower EYFP excitation range prevents bleed-through in the tdTomato channel.

## **3.2 Morphological description of the VIP-expressing interneuron cell body and nucleus**

I first analysed the morphology of imaged and reconstructed VIP-expressing interneurons. Two sections of one VIPcre-tdTomato mouse could be imaged, yielding 4 reconstructed VIP+ cells (fig. 9). Their cell bodies have an average volume of  $583.064 \pm 71.658 \mu\text{m}^3$  (table 1). Somata are largely round to slightly oval, and have very few, large dendrites (fig. 9A). Imaged cells have bipolar or bitufted structures, which is typical for VIP+ interneurons. A striking common characteristic of VIP+ neurons is the highly irregular shape of their nuclei, as can be seen in the EM images and in the resulting 3D reconstruction (fig. 9B, C). The nuclei appear elongated, with complex foldings and rough textures on their membranes. All imaged VIP+ cells have this irregular nucleus.

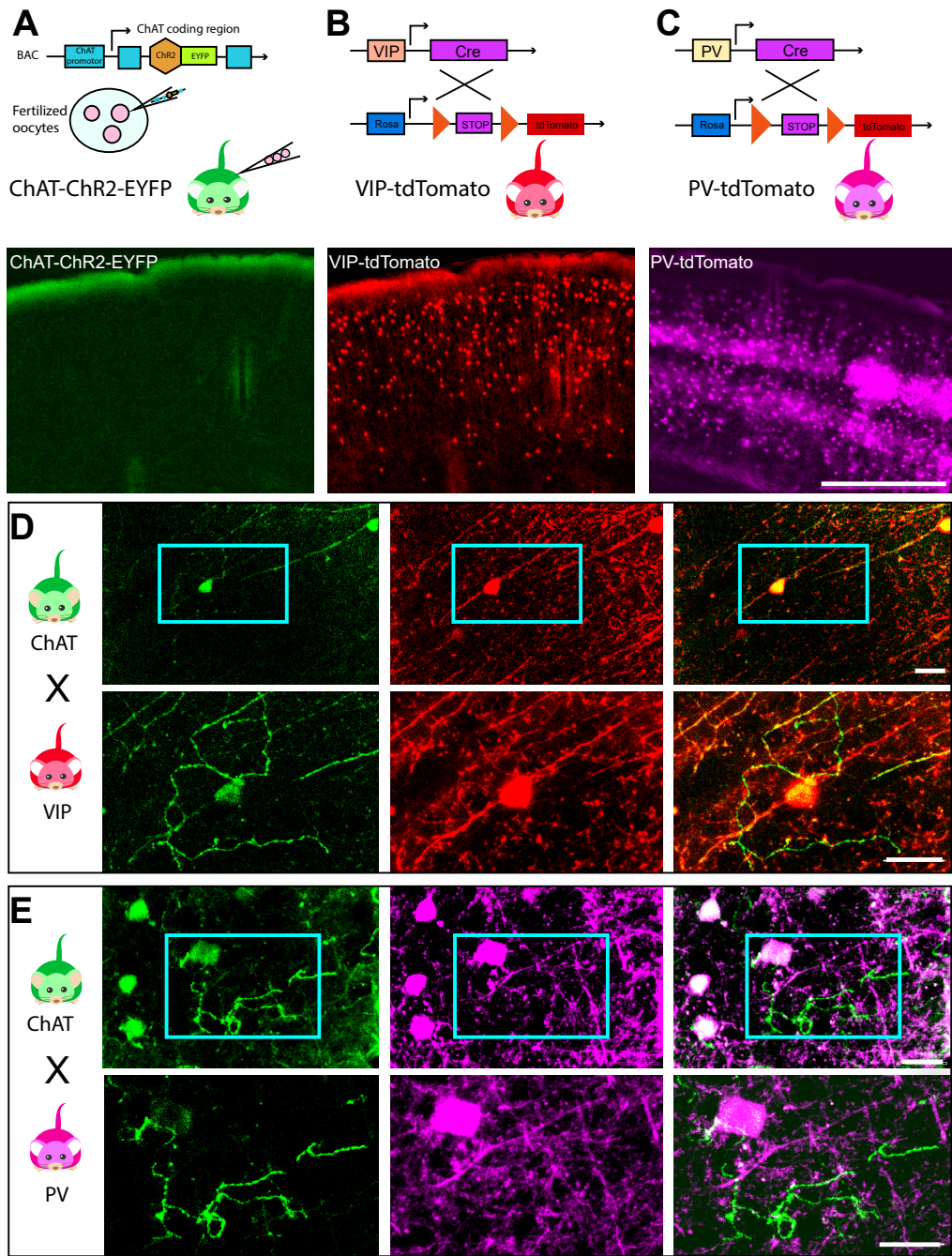


**Figure 8: Illustration of the transgenic mice lines used for my study. (A-C)** Schematic illustration of the genetic manipulations performed to obtain ChAT-ChR2-EYFP, VIP-ires-tdTomato and PV-ires-tdTomato mice lines with their respective low magnification fluorescent images (80  $\mu\text{m}$  thick brain slices at 10X magnification, scale bar = 500  $\mu\text{m}$ ). **(D)**. Confocal images at 20X (upper panel) and 40X (lower pannel) of a VIPcre-tdTomato/ChAT-ChR2-EYFP mouse. **(E)** Confocal images of PVcre-tdTomato/ChAT-ChR2-EYFP mouse at 20X (upper panel) and 40X images (lower panel). Scale bars = 20  $\mu\text{m}$ .

**Table 1: Quantification of cell body volume of four imaged and reconstructed VIP+ cells.**

Cell number	Cell body volume ( $\mu\text{m}^3$ )
VIP1	523.841
VIP2	695.598
VIP3	518.021
VIP4	594.797
VIP average	583.064 $\pm$ 71.658

### 3.3 Morphological analysis of VIP-expressing interneurons' dendrites

As mentioned in chapter 1.2, VIP+ cells can have a bipolar or bitufted structure, with one or two large dendrites that show limited branching. A bitufted morphology can be observed in all imaged cells (fig. 10 A,B). As the vasointestinal peptide is a cytoplasmic marker and its distribution is not limited to the soma, VIP-positive dendrites whose somata are outside the field of view (FOV) can be imaged and reconstructed. This offers the possibility to compare proximal dendrites (cell body in the FOV) with distal dendrites (soma outside the FOV). Synaptic connections on proximal and distal dendrites were mainly found on the dendritic shaft but a few were formed via spines, small membrane protuberances (fig. 10C). Spines on proximal VIP+ dendrites have an average neck length of  $0.4 \mu\text{m}$  and an average head volume of  $0.1 \mu\text{m}^3$ . However, there are no spines on the analyzed distal dendrites. Overall,  $214 \mu\text{m}$  of proximal and  $86 \mu\text{m}$  of distal dendrites could be reconstructed (table 2). The analysis of synaptic contacts reveals that VIP dendrites generally have more excitatory than inhibitory synapses. However, this relation differs drastically between proximal and distal dendrites. The ratio between excitatory and inhibitory synapse frequencies (i.e. how many synapses you would on average expect on  $1 \mu\text{m}$  of dendrite) can serve as an indicator of the relative importance of excitatory and inhibitory input (see chapter 2.7). Whereas proximal dendrites have an excitatory input ratio of 25.5 (i.e. proximal dendrites have 25 times more excitatory than inhibitory synapses), distal dendrites have a ratio of only 5 (table 2). GABAergic and glutamatergic synapses appear to have similar sizes (fig. 10D), thus a similar trend is visible when

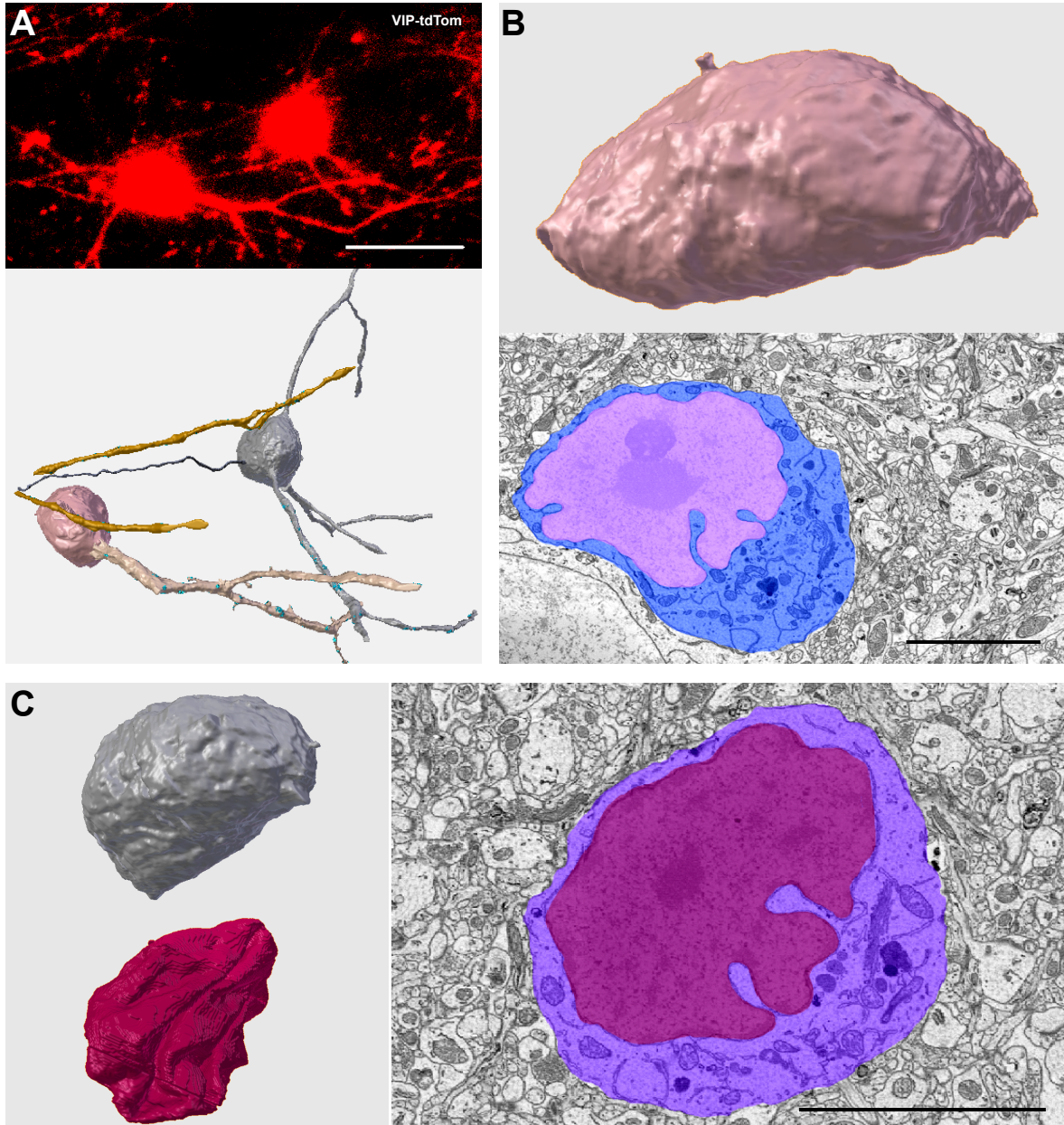


**Figure 9: Morphologic description of the VIP-positive interneuron's cell body.**  
(A) Z-projection of a stack of confocal images of VIP-tdTomato/ChAT-ChR2-EYFP showing the 2 VIP+ cells and corresponding 3D EM reconstruction. Scale bar = 20  $\mu\text{m}$ . (B) 3D EM reconstruction and EM image of the left VIP+ on the left showing its nucleus and cell body features. (C) 3D EM models (left top and bottom) and EM image (right) of the VIP+ cell body and nucleus. EM scale bars = 5  $\mu\text{m}$ .

considering synaptic surface instead of synapse numbers, with proximal dendrites having a ratio of 13.71 versus 5.17 for distal dendrites (table 2). However, distal synapses appear to be smaller than contacts on proximal dendrites, although this trend is not statistically significant ( $P = 0.051$ , two-way ANOVA,  $F(1,167)=3.858$ , fig. 10D).

**Table 2: Analysis of proximal and distal VIP+ dendrites.** Data pooled from X proximal dendrites belonging to 4 reconstructed VIP+ neurons and Y distal dendrites belonging to an unknown number of VIP+ cells. Proximal dendrites have their soma in the field of view, whereas distal dendrites have their soma outside. Formulas for input ratios are described in chapter 2.7.

Measurement	Proximal	Distal
N. excitatory synapses	110	47
N. Inhibitory synapses	4	10
Dendrite length [ $\mu m$ ]	214.196	86.266
Excitatory surface [ $\mu m^2$ ]	27.07	8.86
Inhibitory surface [ $\mu m^2$ ]	1.98	1.72
Dendrite surface [ $\mu m^2$ ]	564.35	203.90
Excitatory frequency [ $\mu m^{-1}$ ]	0.51	0.55
Inhibitory frequency [ $\mu m^{-1}$ ]	0.02	0.11
Excitatory input ratio (N. syn.)	25.50	5.00
Excitatory surface ratio [%]	4.80	4.34
Inhibitory surface ratio [%]	0.35	0.84
Excitatory input ratio (area)	13.71	5.17

### 3.4 Morphological description of the PV-expressing interneuron cell body

Next, I reconstructed and analysed parvalbumin-expressing interneurons. One section of one mouse expressing tdTomato in all PV+ neurons could be analysed, where one PV+ cell was imaged and reconstructed.

In contrast to the more regular, bipolar structure of the VIP neurons, the PV+ neuron has a rounder soma with several, highly branching dendrites extending in all directions (fig. 11B, C). With  $1555.29 \mu m^3$ , the PV+ cell is nearly three times larger than the

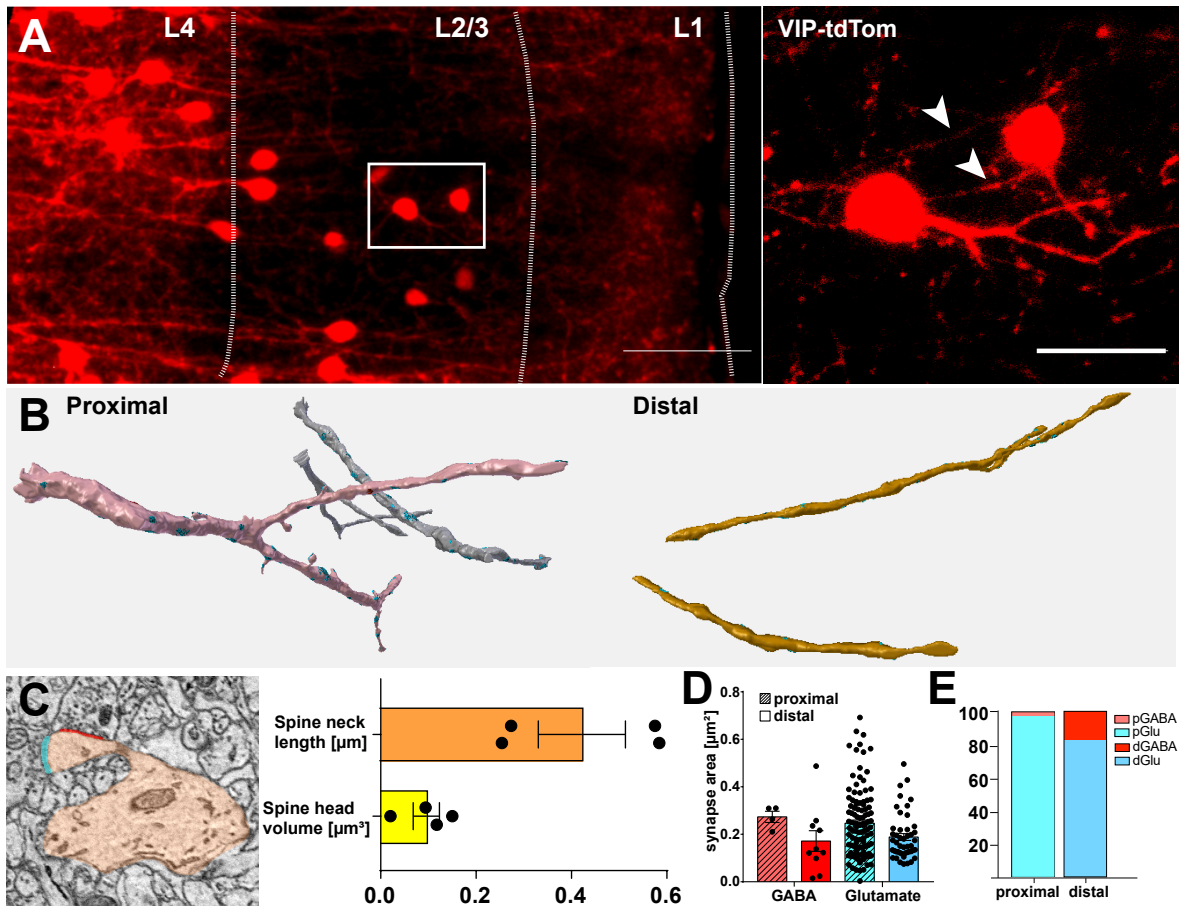


**Figure 10: Comparison of VIP+ proximal and distal dendrites.** (A) Representative fluorescent images at low (10X, left) and high (40X, right) magnification of VIP+ cells. Scale bars = 50 (left) and 20 (right)  $\mu\text{m}$ . (B) 3D EM reconstructions of proximal (left) and distal (right) VIP+ dendrites. (C) Representative EM image of a proximal VIP+ spine with inhibitory (blue) and excitatory (red) synapse. Quantification of VIP+ spine head volumes and spine neck length ( $n = 4$ ). (D) Excitatory and inhibitory synapse sizes on proximal and distal dendrites. Two-way ANOVA,  $F(1,167)=3.858$ ,  $P=0.051$ . N listed in table 2. (E) Relative abundance of inhibitory (red) and excitatory (blue) synapses on proximal and distal synapses.

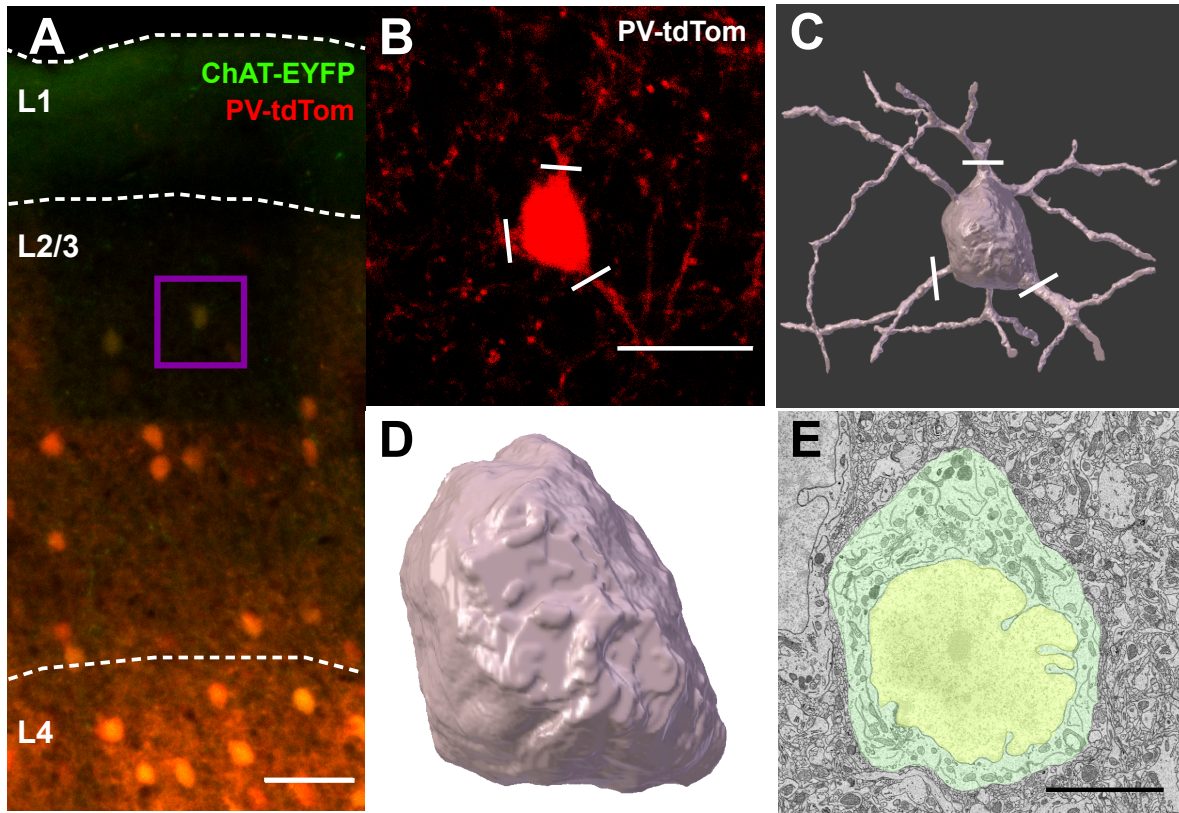


**Figure 11: Cell body and nucleus of a PV+ interneuron.** (A) 10x confocal overview of PV expression in S1. Square shows ROI with reconstructed cell. Scale bar =  $\mu\text{m}$ . (B and C) 40x confocal image of the reconstructed PV+ cell and corresponding 3D EM reconstruction. Main dendrites are marked with lines. Scale bar = 20  $\mu\text{m}$ . (D and E) 3D EM reconstruction and EM image of PV+ soma and nucleus. Scale bar = 5  $\mu\text{m}$ .

VIP+ neurons. Its nucleus is shaped irregularly, similar to the nuclei of the VIP+ cells, with deep foldings, but a more round shape (fig. 11D, E).

### 3.5 Morphological analysis PV-expressing interneuron dendrites

As mentioned before, multiple ( $n = 6$ ) dendrites of the PV+ neuron emerge from the soma in all directions and form branches repeatedly, giving the cell a ramified shape (fig. 9C, 12). Overall, dendrites with a total length of  $\sim 327 \mu\text{m}$  and a surface of  $1799 \mu\text{m}^2$  were analyzed. Similarly to VIP+ cells, PV+ dendrites receive more excitatory than inhibitory input (table 3), although the ratio is not as skewed as in the

VIP+ cells. Furthermore, the average synapse size is relatively small, with excitatory synapses measuring  $0.15 \mu m^2$ . Inhibitory synapses are with  $\sim 0.08 \mu m^2$  even smaller ( $P < 0.001$ , fig. 12F). All analyzed synaptic connections occur directly on the dendritic shaft (fig. 12B). Only 2 membrane protrusions are observed on PV+ dendrites with spine head volumes of  $0.4 \mu m^3$  and  $0.01 \mu m^3$ . Furthermore, none of the spines form synaptic contacts. In combination with the extremely small size of the second spine, it is difficult to assess whether it may be a still developing spine or a random membrane protrusion. Spine neck length is  $\sim 1 \mu m$  for both spines. Unfortunately, no distal PV+ dendrites could be identified, and a comparison similar to chapter 3.3 is not possible.

**Table 3: Quantification of synaptic input on PV+ dendrites.**

Num. ex. syn.	Num. inh. syn.	Dend. length	Ex. freq.	Inh. freq.
309	42	$327.487 \mu m$	$0.94 \mu m^{-1}$	$0.13 \mu m^{-1}$
Ex. surface	Inh. surface	Dend. surface	Ex. ratio (%)	Inh. ratio (%)
$46.895 \mu m^2$	$9.000 \mu m^2$	$1799.022 \mu m^2$	2.60	0.50

### 3.6 Morphological analysis of ChAT-expressing axons

Next, the acetyl cholinergic axons found in the region of interest were reconstructed. A total of  $333.78 \mu m$  of 7 cholinergic axons from two independent experiments were analyzed (fig. 13A). These elements are relatively thin with enlargements where the vesicles accumulate, highly ramified and unmyelinated (fig. 13 B and C). To assess the cholinergic output, regions contacting dendritic shafts or spines with 3 or more vesicles were considered functional contacts (fig. 13 C). The contact surface area ( $\sim 0.08 \mu m^2$ ) was consistent across experiments. A contact density of 0.16 synapse per  $\mu m$  axon length was observed (table 4).

**Table 4: Morphological quantification of ChAT+ axons in the barrel cortex.** Ratios show number of contacts per  $\mu m$  (column 4) or relative axon surface occupied by membrane contacts (column 7). Data pooled from 7 reconstructed axons from 2 sections.

	N. cont.	Axon length	Ratio	Cont. surf.	Axon surface	Ratio
ChAT-VIP	24	$214.22 \mu m$	11.2	$2.47 \mu m^2$	$370.56 \mu m^2$	0.67 %
ChAT-PV	31	$119.56 \mu m$	25.6	$2.21 \mu m^2$	$241.87 \mu m^2$	0.91 %
Total	55	$333.78 \mu m$	16.48	$4.68 \mu m^2$	$612.43 \mu m^2$	0.76 %

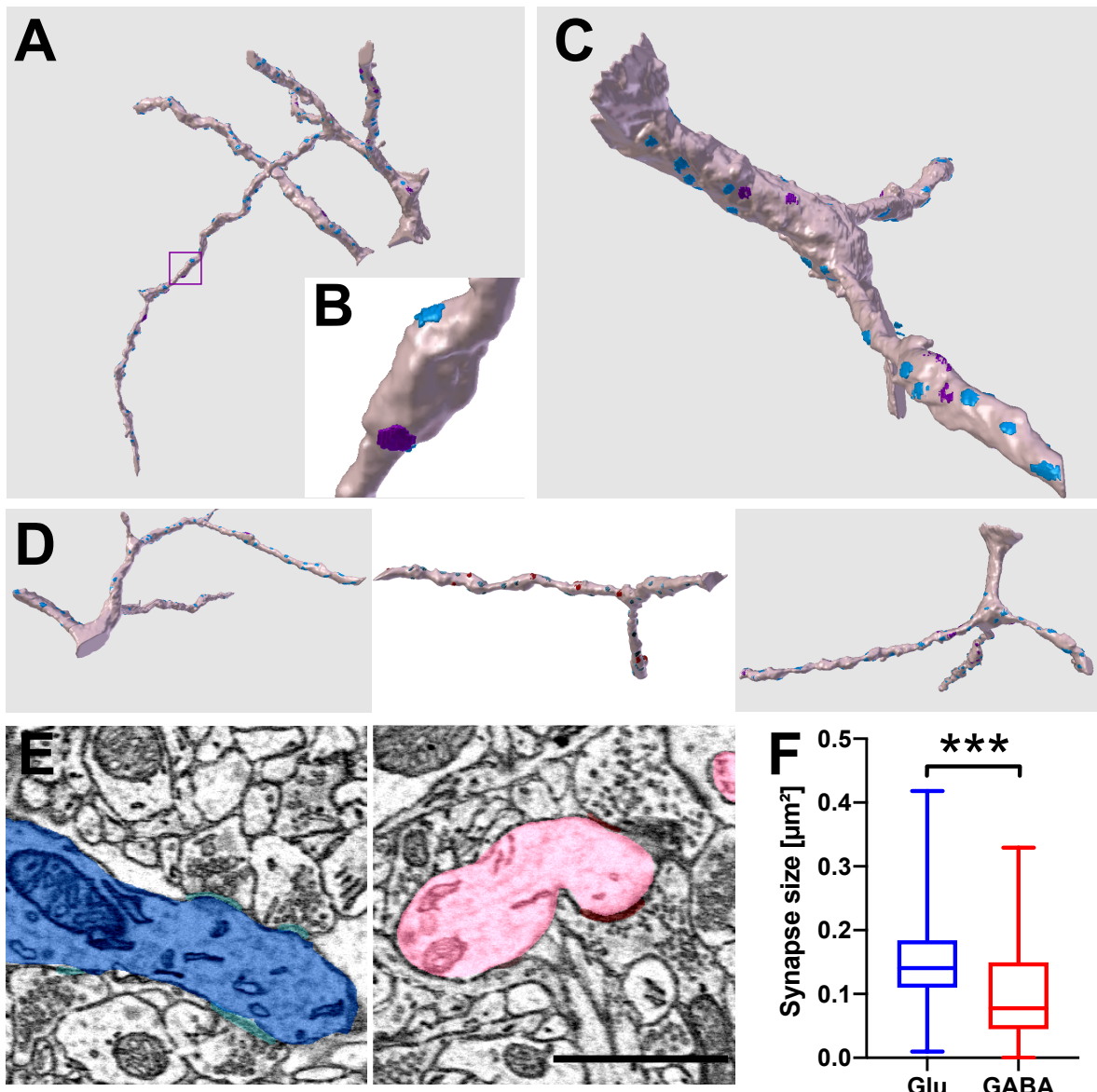


**Figure 12: Analysis of synaptic input onto proximal PV+ interneurons.** (A) Complete 3D EM reconstruction of a PV+ dendrite. (B and C) High magnification and overview of reconstructed synapses on the dendritic shaft of a PV+ dendrite. (D) Reconstructions of the other 4 PV+ dendrites. (E) Representative EM images of excitatory (left) and inhibitory (right) synapses (scale = 1  $\mu\text{m}$ ). (F) Distribution of the glutamatergic and GABAergic synapse surface area. Unpaired Student's t-test,  $t=4.884$ ,  $df=349$ ,  $P<0.001$ . Normal distribution confirmed before with Kolmogorov-Smirnov test ( $P<0.001$ ).

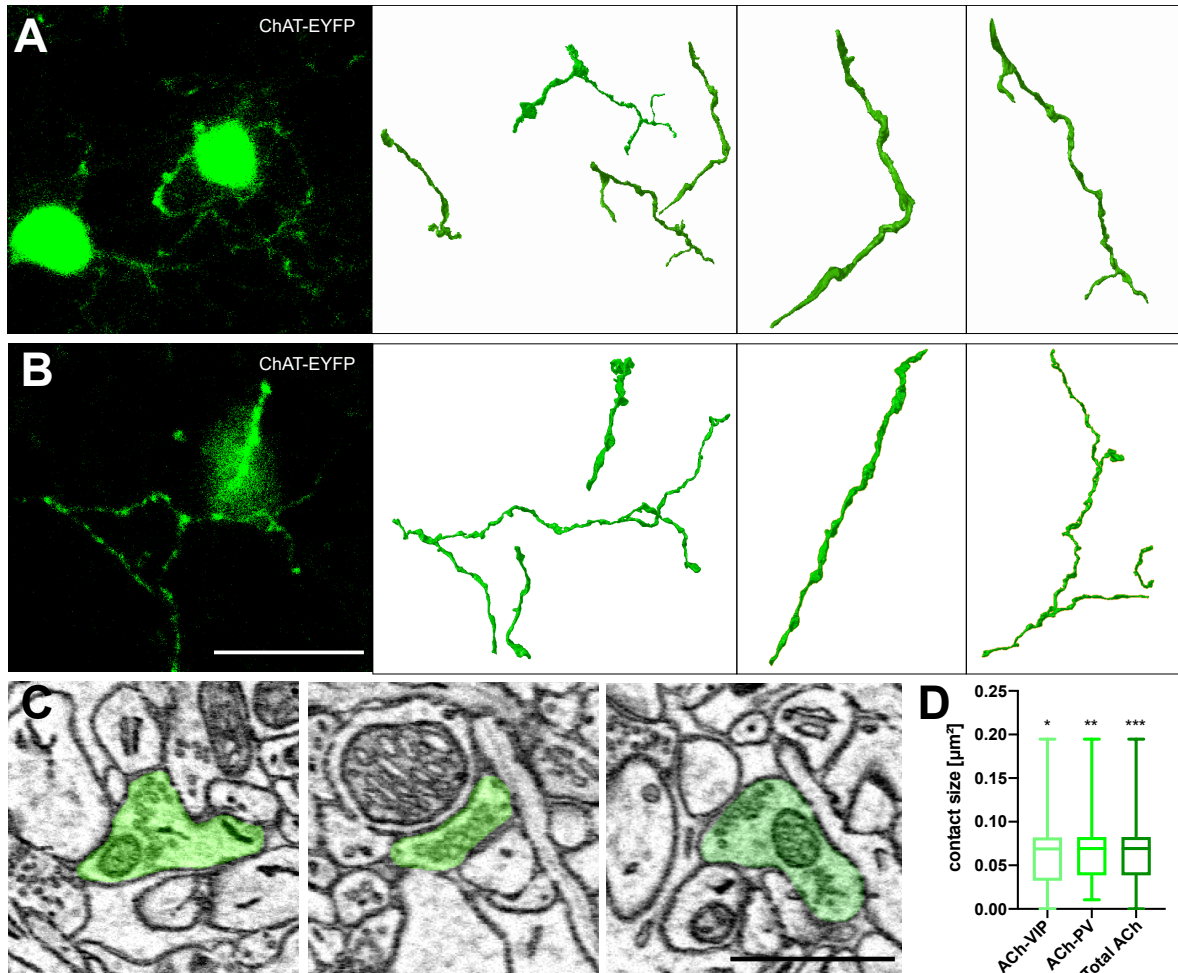


**Figure 13: ChAT-positive axons.** (A and B) Fluorescent images of ChAT+ axons in the VIP (A) and PV (B) experiment as well as their 3D EM reconstructions (middle: overview, right: single axons). Scale bar = 20  $\mu\text{m}$ . (C) Representative EM images of cholinergic axons apposing other structures. Scale bar = 5  $\mu\text{m}$ . (D) Quantification of the ACh contact size to VIP+ and PV+ neurons. Asterisks show P-values of Kolmogorov-Smirnov test for normal distributions.

## **3.7 ChAT-expressing axons and their interaction with GABAergic interneurons**

### **3.7.1 VIP+ interneurons and ChAT+ axons interaction**

First I assessed the interaction between VIP-expressing cells and cholinergic axons in layer II/III of barrel cortex (fig. 14). Ultrastructural EM imaging and subsequent 3D reconstruction showed that ChAT-positive axons contact VIP+ cell body and dendrites in a synaptic and non-synaptic manner (fig. 14D, E and F). These contact are observed also onto distal dendrites (fig. 14C). The contact surface between the two structures of interest was quantified grouped per VIP+ cell body, proximal and distal dendrites (fig. 14G). According to my measurement, the proximal dendrites have a larger absolute contact surface ( $\sim 0.52 \mu m^2$ ) than the cell body and distal dendrites. However, when considering the smaller membrane surface of the distal dendrites, the ACh contacts cover nearly double the area on distal compared to proximal dendrites. ( $\sim 0.18 \%$ , fig. 14G).

### **3.7.2 PV+ interneurons and ChAT axons interaction**

In this experiment a PV+ cell of layer II/III and the cholinergic axons in its proximity were reconstructed and analyzed (fig. 15). Even though the cholinergic axon have higher synaptic output in this region, 25.6 %, compared to 11.2 % in the region of VIP+, (table 4), here only one ChAT/PV contact with ACh vesicles was found, located on the PV+ cell body (fig. 15). Surprisingly, no ChAT+ contact was found within the  $\sim 327 \mu m$  of PV+ dendrites (table 3). However, the single contact found on the cell body shows no clear synapse, indicating that ChAT+ axon have a lower tendency to contact PV+ cells then VIP+ cells.

## **3.8 VIP+ and PV+ axons characterization**

It was possible to identify and reconstruct the axon of one VIP+ and one PV+ cell. Several differences are apparent between the axons of these cell types (table 5). The VIP+ axon is extending relatively straight from the soma, without branching (fig. 16A). Additionally, the axon formed two synaptic outputs in the reconstructed region (fig. 16 Ac, Ad). At the place of the contact, the axon increases in diameter and

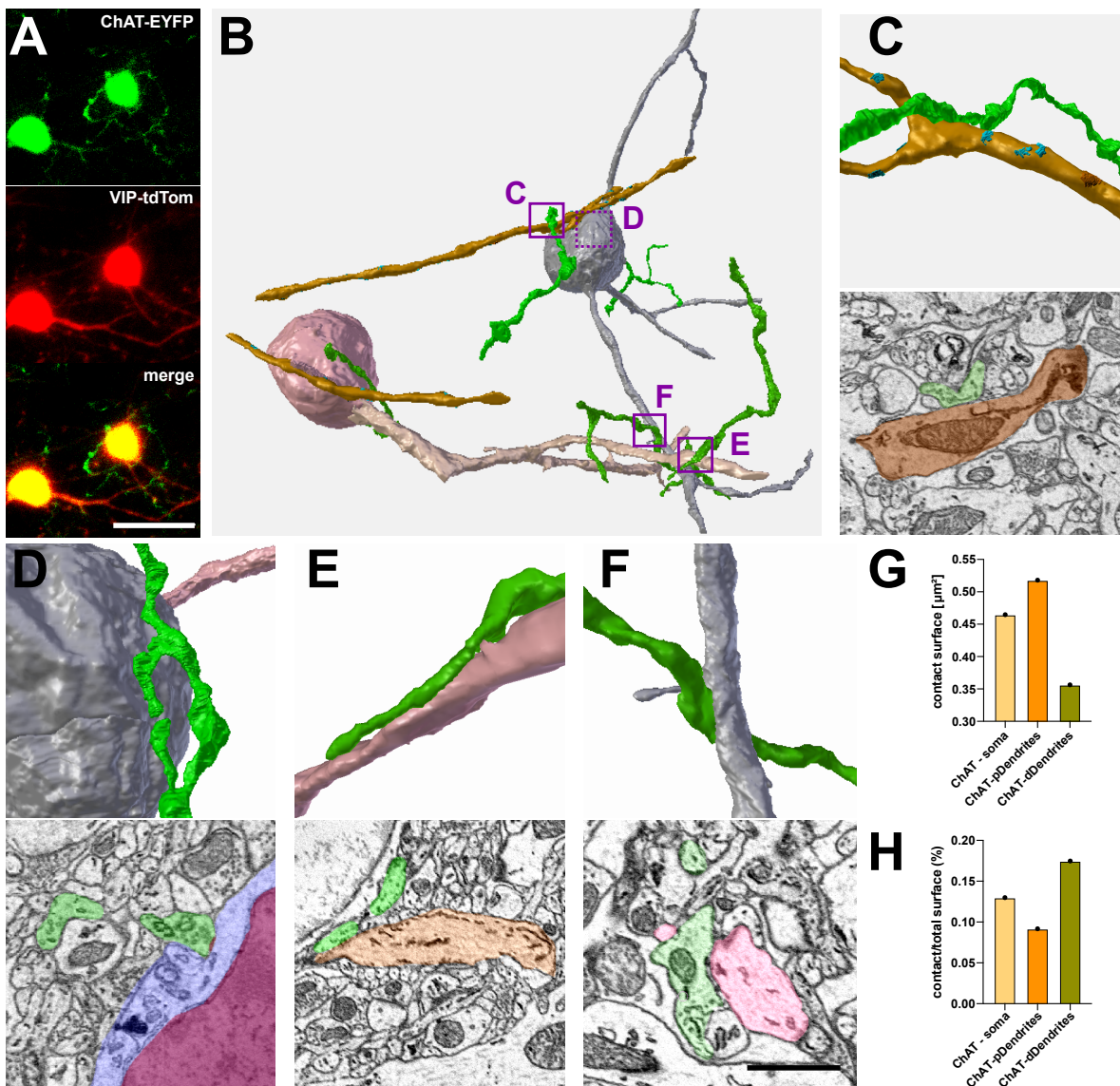


**Figure 14: VIP-positive interneurons and acetyl cholinergic axons interaction.** (A) ChAT+ axons (top), VIP+ neurons (mid) and merged confocal 40x images (bottom). Scale bar = 20  $\mu\text{m}$ . (B) 3D EM reconstructions of VIP+ neurons and surrounding ChAT+ axons seen in A. Boxes and letters indicate contact locations shown in C-F. C-F 3D reconstructions and EM micrographs of contacts between ChAT+ axons and VIP+ proximal dendrites (E and F), distal dendrites (C) and soma (D). (G and H). Quantification of ChAT-VIP interaction in different regions of the neuron, as measured in total contact surface (G) and relative contact surface (H) normalized against total axonal surface.

accumulates vesicles (fig. 16 Ad). In contrast, the PV+ axon is more irregular. It curves back about 120° shortly after emerging from the soma and branches multiple times (table 5, fig. 16 B). As opposed to the unmyelinated VIP+ axon, the PV+ axon

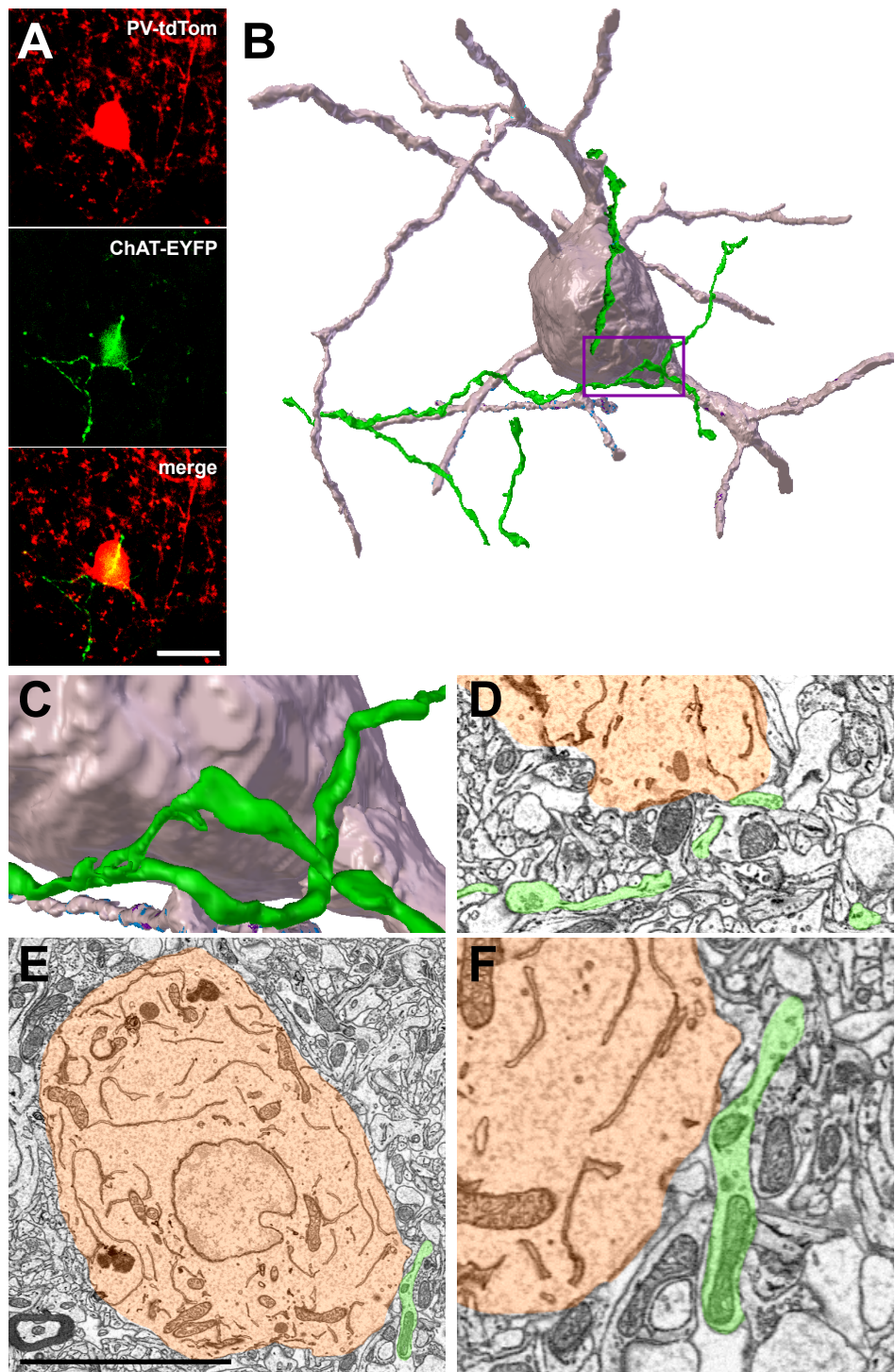


**Figure 15: PV-positive interneuron and cholinergic axon interactions.** (A) Representative fluorescent images of a PV+ cell (top), an adjacent ChAT+ axon (mid) and merged channels (bottom). Scale bar = 20  $\mu$ m. (B) 3D EM reconstruction of the imaged PV+ cell and the ChAT+ axon in close proximity, indicated by the box. (C-F) 3D reconstruction and EM micro of ChAT+/PV+ contacts. Scale bar = 5  $\mu$ m.

is surrounded by thick myelin sheets (fig. 16 Ba,b), and does not form synapses nor accumulates vesicles.

**Table 5: Morphological quantification of VIP+ and PV+ interneuron axons.** One VIP+ and one PV+ axon were quantified. Axon length shows the length of axons in the FOV that could be reconstructed and analysed.

Cell type	Axon length (analyzed)	Synaptic output	Myelinated	Branches
VIP+ IN	42.29 $\mu m$	2	No	None
PV+ IN	171.96 $\mu m$	0	Yes	4

### 3.9 Cilium characterization

Surprisingly, two VIP+ and one PV+ cell have a cilium each, protruding from the soma (fig. 17). The cilia are 8 – 11  $\mu m$  long (table 6) and are recognizable by the characteristic 9x2+0 arrangement of microtubules typical for non-motile primary cilia (fig. 17A). All reconstructed cilia have a rather regular structure with only minor curves.

**Table 6: Morphological quantification of cilia on VIP+ and PV+ cells.** 2 VIP+ cells and 1 PV+ each present one cilium that could be reconstructed.

Cell type	Cilium length ( $\mu m$ )
VIP+	11.065
	9.904
PV+	8.036

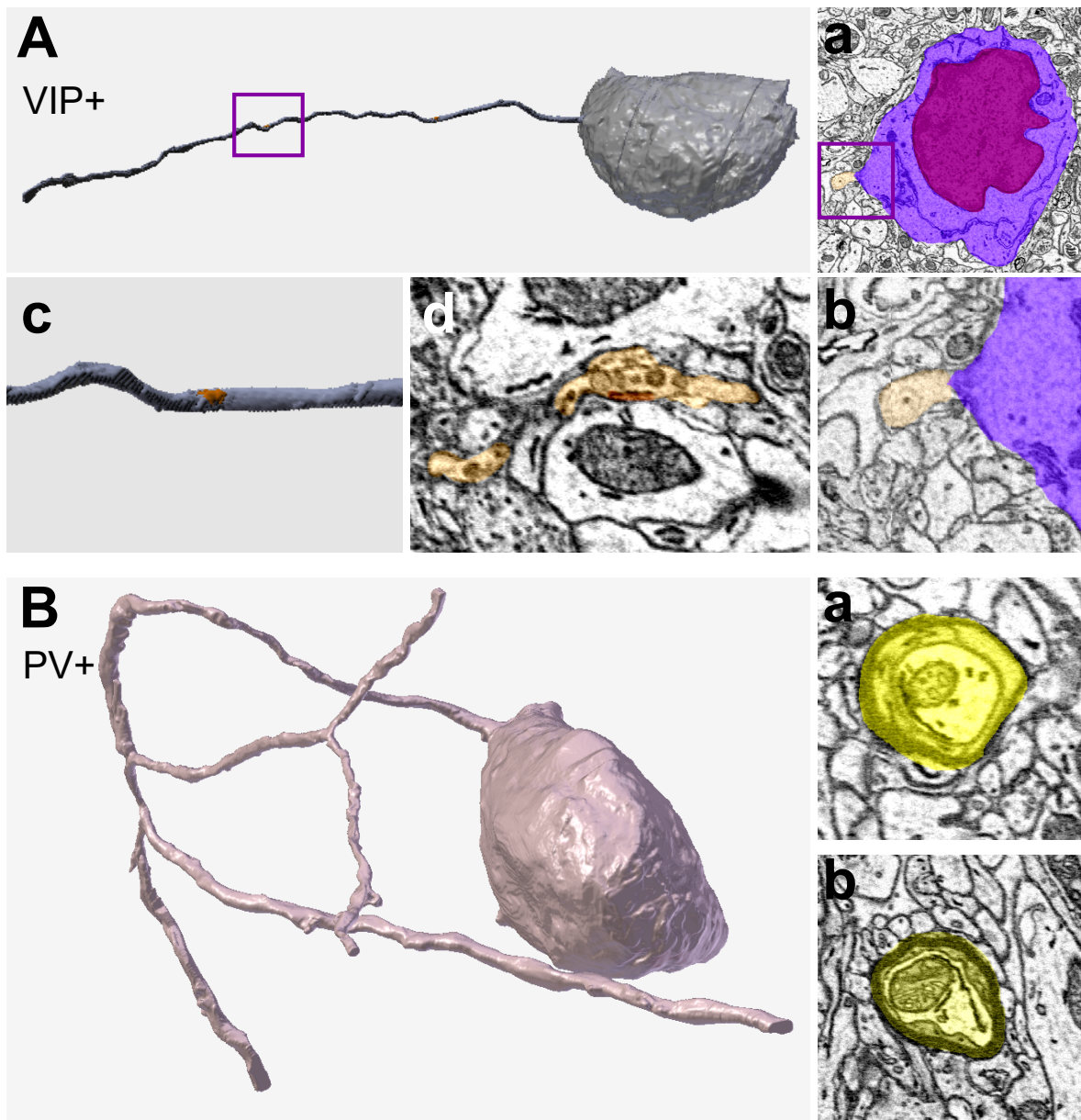


**Figure 16: 3D reconstruction of VIP+ and PV+ axons.** (A) Representative image of a VIP+ axon. (a and b) Representative EM images of the axon emerging from the cell body. (c and d) 3D reconstruction and EM images of a synapse found on the VIP+ axon. (B) EM reconstruction of a PV+ axon. (a and b) Representative EM images of the myelinated PV+ axon. Boxes indicate locations of zoom.

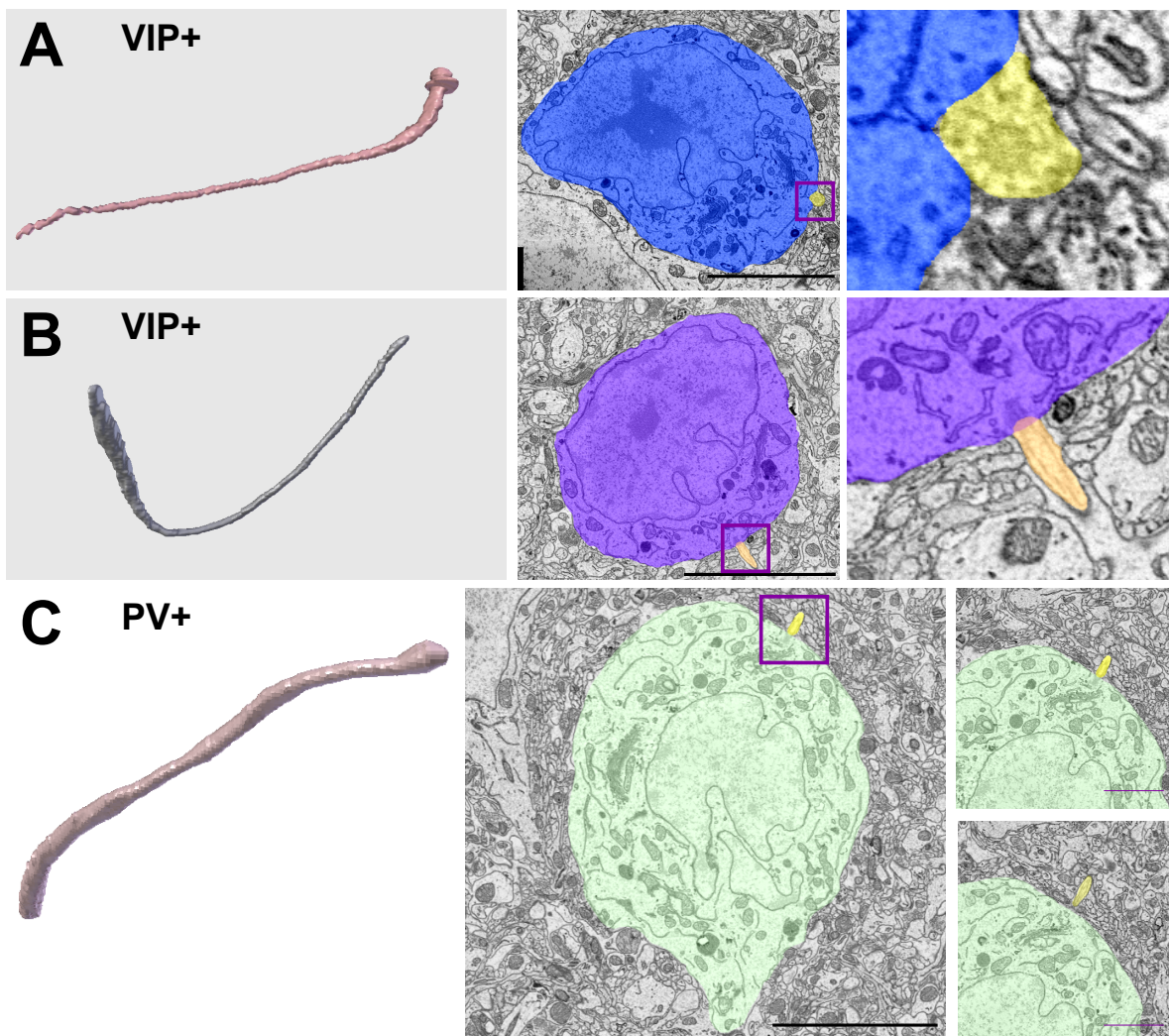


**Figure 17: 3D reconstruction and EM micrographs of VIP+ and PV + cilia**  
3D EM reconstructions, EM images of the whole cell and high magnification of cilia emerging from VIP+ cells (**A and B**) and a PV+ cell (**C**). Boxes indicate location of zoom. Scale bars = 5  $\mu m$  for low magnification and 1  $\mu m$  for high magnification micrographs.

# **4 Discussion**

## **4.1 Small sample size limits significance**

As stated previously, the data that could be gathered during this project is originating from a very limited sample size. In total, 4 VIP+ neurons from 2 mice, 1 PV+ cell as well as 7 ChAT+ axons from 2 mice were reconstructed. Whereas the quality of the dataset itself is not affected, this small sample size makes it difficult to generalize our findings to the whole population of the investigated cell types. One has to bear this in mind when drawing conclusions from the results presented here.

## **4.2 VIP+ and PV+ soma and nuclei are irregularly shaped**

In this project, we imaged and reconstructed 4 VIP+ and 1 PV+ interneuron in layer II/III of the rodent barrel cortex. Through reconstructing cells imaged with a scanning electron microscope to digital 3D models, we observe that VIP+ cells appeared to be more elliptic (not measured directly) and smaller in size compared to PV+ cells. More specifically, the PV+ soma has a volume three times higher than the VIP+ neurons. In both cases the nuclear membrane foldings were observed (fig. 9, 11). Neuronal nuclei have been shown to change their morphology according to the activity of N-methyl-D-aspartate receptors (NMDARs, Wittmann et al. (2009)), as membrane foldings are indicators of an elevated interaction between endoplasmic reticulum (ER) and the nucleus. NMDARs are well known to drive long term plasticity (LTP) in neurons, where activation of NMDARs leads to increased calcium influx at the postsynapse, which in turn activates signalling cascades inducing new protein synthesis (Malenka, 1991). Therefore, our results suggest that these cell types could have a high synaptic activity and plasticity, indicating an important role in the modulation of the activity of the microcircuit in which they are situated. It would be interesting to understand if

more finely grained structural details like ER arrangements around the nucleus are also present, and whether these features are also found in other interneurons with similar disinhibitory roles, such as SST+ cells. Unfortunately, this was outside the scope of this project.

### 4.3 VIP+ and PV+ dendrites receive excitatory and inhibitory input

We analyzed around 300 (proximal and distal) and 327  $\mu\text{m}$  of VIP+ and PV+ dendrites respectively (fig. 10, 12, table 2, 3). Synapse reconstructions revealed a higher excitatory than inhibitory input for both cell types. These synapses are generally found on the dendritic shaft, and few spines were reconstructed (total n = 5, 4 VIP+, 1 PV+), indicating that these cells are aspiny neurons (fig. 10, 12). Furthermore, analysis of synapses on the proximal and distal VIP+ dendrites revealed substantial disparities in their synaptic input in terms of the proportion of excitation to inhibition. The inhibitory inputs, although slightly smaller than the excitatory inputs, are more abundant on distal compared to proximal dendrites (fig. 10E, table 2). In fact, total excitatory input (as measured as the ratio between excitatory and inhibitory synapse numbers) is 25 times greater than inhibitory input for proximal and 5 times greater for distal dendrites, a 5-fold difference between proximal and distal dendrites (table 2). While this analysis is based on synapse numbers, the conclusion holds when calculating the ratio of excitatory versus inhibitory synapse sizes, although the result of a 4-fold difference (table 2) is somewhat less pronounced.

This variation in the inhibitory input suggests a high targeting specificity of axons from different origins. Proximal dendrites are mainly responsible for the generation of action potentials (APs), as they are closer to the axon hillock. The hillock is considered the AP-generating region of the soma, thus synaptic currents on proximal dendrites have a larger influence on the AP generation by being more closely located to the axon hillock (Palay et al., 1968; Wollner and Catterall, 1986; Haeusser et al., 2000). Synapses on the distal dendrites however have more modulatory function, indirectly related to APs. They instead influence the activity of the postsynaptic neuron by silencing or disinhibiting regions of the dendritic membrane. These results suggest that even inhibitory interneurons - being themselves modulatory for principal neurons – receive dense modulating inhibitory input, supporting the theory of local disinhibitory circuit motifs as

an essential aspect of cortical networks (Pfeffer et al., 2013; Pfeffer, 2014).

## **4.4 Comparing synapse sizes of proximal and distal VIP+ and PV+ dendrites**

Classically a synaptic connection is defined as a specific structure with a pre-element containing neurotransmitter vesicles, and a post-element receiving the neurotransmitter. Glutamatergic and GABAergic synapses have been well characterized and are easily recognizable on EM images. However, the modulatory connections are not as well defined. In our case, we traced glutamatergic and GABAergic synapses on proximal/distal VIP+ and PV+ dendrites (ch. 3.3, fig. 10, 12).

We found that proximal GABAergic and glutamatergic synapses on VIP+ cells have comparable surface area (respectively  $0.27 \pm 0.04$  and  $0.25 \pm 0.14 \mu\text{m}^2$ , fig. 10D). Similar observations were made also on the distal dendrites where the GABAergic and the glutamatergic synapses have a surface area of  $0.18 \pm 0.13$  and  $0.19 \pm 0.10$  respectively. However, when proximal and distal synapse size were compared between each other, we saw a reduction in size of the synaptic surface, with a significant difference between proximal and distal glutamatergic synapses.

Similarly, PV+ dendrites form both GABAergic and glutamatergic synapses (table 3). In contrast to VIP+ neurons, the surface areas of GABAergic and glutamatergic synapses on PV+ cells are significantly different (ch. 3.5, fig. 12), suggesting that there might a higher release of glutamate. However, substantiating this hypothesis will require further analysis and recordings with higher resolution to more accurately identify and reconstruct synapse types.

## **4.5 Cholinergic axons form synapse-resembling connections**

The barrel cortex is supplied with acetylcholine mainly by cholinergic axons projecting from the nucleus basalis (Ch4 or basal forebrain, fig. 3). However, local cortical interneurons have been shown to express ChAT, with 98% of this cortical cholinergic population coexpressing VIP (fig. 18, Gonchar et al. (2008)). This phenomenon would partially explain why we observe a substantial amount of VIP+/tdTomato signal in

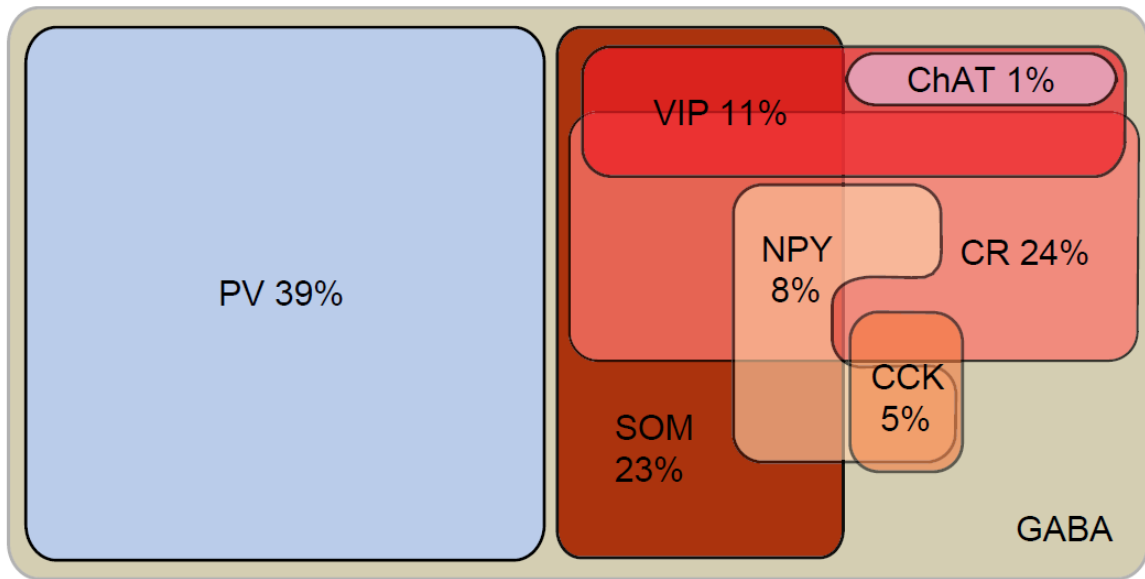


**Figure 18: Protein expression of cortical interneuron populations.** Relevant for this study is the expression of ChAT in GABAergic interneurons. As can be seen in this graphic, ChAT is only expressed by GABAergic interneurons exclusively in co-expression with VIP. From Gonchar et al. (2008).

the ChAT/EYFP channel (fig. 13A, 14A). This is enhanced by overlapping excitation spectra of EYFP and tdTomato. For our study, we focused on axons that emitted only in the EYFP channel, which should eliminate 98% of local cholinergic interneurons. We can thus be fairly confident that the reconstructed ChAT+ axons are originating from the basal forebrain and are not ChAT-expressing VIP+ cells. The analyzed ChAT+ axons showed previously reported features. They are thin, unmyelinated, highly ramified and form vesicle-accumulating varicosities (Descarries and Mechawar, 2000). The ChAT+ axons were analyzed with the focus to understand how they are acting on other cortical elements. There is an increasing interest in understanding these mechanisms because recent studies have shown that acetyl choline is involved in the GABAergic interneurons circuitry modulation (Fu et al., 2014). Specifically, ACh is hypothesized to enhance the VIP+ activity which inhibits SST+ interneurons. The SST+ cells innervate the distal dendrites of pyramidal cells (PCs), therefore their inhibition results in a disinhibition of excitatory PCs, causing a net increase in excitatory network activity (fig. 4). Moreover, functional studies have shown a rapid transmission mechanism suggesting that the cholinergic axons might make direct contacts with the VIPs. Studies have reported evidence for both volume transmission and synaptic contacts of ChAT+ axons (Sarter et al., 2009). Our findings confirm that ChAT+ axons are very closely

associated with interneurons, but we were not able to clearly identify true synapses. However, we observed appositions of the cholinergic axons onto dendritic shafts and spines (fig. 13C). Although these structures do not perfectly resemble classic synapses with a synaptic cleft, pre- and post-synaptic densities and docked vesicles on the pre-synaptic membrane, we still observe these features albeit less accentuated. In fact, these synapse-like contacts present a smaller surface area ( $\sim 0.085 \mu\text{m}^2$ ) and are less frequent (0.16 contacts/ $\mu\text{m}$  (table 4) than GABAergic and glutamatergic synapses (tables 2, 3). These synaptic-like structures were found every  $\sim 6 \mu\text{m}$  along the analyzed axons.

## 4.6 ChAT+ axons contact VIP+, but not PV+ interneurons

A question that is still discussed vigorously is the nature of ACh communication with local interneurons (Sarter et al., 2009). Whereas it has been reported that ChAT+ axons are in principle able to form synaptic contacts (Turrini et al., 2001), synapses between ChAT+ axons and GABAergic interneurons have not yet been detected, although communication between them has been shown repeatedly (Wanaverbecq et al., 2007; Pfeffer et al., 2013; Fu et al., 2014; Letzkus et al., 2011). It is thus hypothesized by some that ACh is released via volume transmission rather than through true synapses (Descarries et al., 1997). However, in a recent study conducted by Fu et al. 2014 in the visual cortex, ACh was found to activate the VIP+ cells directly through nicotinic ACh receptors (nAChR). Moreover, some studies reported cholinergic activity onto PV+ interneurons (Letzkus et al., 2011). Here, we attempt to clarify the interaction between cholinergic axons and cortical GABAergic interneurons by co-labelling ChAT and VIP or PV. Correlative light and electron microscopy (CLEM) makes it possible to locate previously imaged cells in EM images without the use of fiducial landmarks or EM staining techniques, both of which considerably impact tissue quality and resolution. CLEM is particularly useful to reconstruct small nanoscale structures such as spines and synapses. This allows us to reconstruct ChAT axons as well as find, identify and analyze contacts between it and VIP+ or PV+ cells.

Along the  $\sim 333 \mu\text{m}$  of reconstructed ChAT+ axons we observed 4 contacts between cholinergic axons and VIP+ cells. We found membrane approximations at the level of the cell body, proximal and distal dendrites (fig. 14). However, these contacts are

not clearly synaptic-like. Postsynaptic densities are missing, although varicosities accumulate neurotransmitter in large numbers of vesicles (fig. 14E,F). While here ACh would be released via volume transmission, due to the proximity of the VIP+ cell it is possible that it would receive most of the transmitter, providing a certain spatial specificity to the volume transmission.

In contrast to the contacts observed between ChAT+ axons and VIP+ cells, no such connection was found on the PV+ neuron. Although the ChAT+ axon was found to be directly adjacent to the PV+ soma, no vesicle accumulation was detected in this area. Thus, a functionality of this tangent is unlikely. This finding would corroborate the proposed disinhibitory circuit (fig. 4, Pfeffer et al. (2013)) as well as previous studies showing an effect of ACh on VIP+ neurons, but neither PV+ nor SST+ cells (Alitto and Dan, 2013).

## 4.7 ECS shrinkage might influence neuronal contact morphology

VIP+ cells have been shown to directly contact ChAT+ axons at vesicle-accumulating varicosities (fig. 14). In contrast, we found only one cholinergic axon contacting the PV+ cell body. This region showed no clear vesicle accumulation (fig. 15C-F). These tangent membranes without any synaptic-like structures could be due to fixation artifacts. In fact, it has been well established that the chemical fixation performed for EM imaging causes tissue shrinkage (Boyde and Boyde, 1979). Therefore, extracellular space (ECS) reduction might artificially bring the two elements closer together, without a natural proximity.

Previous analyses of specific types of connections in the CNS have relied on immunocytochemistry where antibodies label the structures of interest (Bopp et al., 2017). Although this method allows the different types of neurons to be easily identified in the tissue, it does not provide optimal preservation of the ultrastructure, as the tissue needs to be treated to provide access for antibodies and stains. This compromises the ultrastructure and leads to nanostructures like synapses being obscured. By using a correlative approach, no specific marking of the axons or dendrites of interest was needed to identify them in the EM, enabling the choice of fixation and EM staining techniques for optimal tissue quality. This meant that any synaptic features, such as vesicles, pre and postsynaptic densities and the synaptic cleft would be clearly visible.

## 4.8 Project outlook

Several possible experiments can be conceived to follow up on this project. Primarily, the low sample size should be increased considerably by imaging and reconstructing more VIP+ and in particular PV+ cells and adjacent cholinergic axons to verify the consistency of these data. Here, most attention should be spent on maximizing the resolution and quality of the EM images to be able to accurately reconstruct and identify the small synapse-like structures and their morphology. Using a focussed ion beam SEM (FIBSEM) instead of the 3View system applied in this project might for example yield better ultrastructural data due to the intrinsically higher resolution of the system. Furthermore, cryofixation instead of chemical fixation might limit shrinkage of the ECS, which would be beneficial for investigating the natural nanostructures of interneuron contacts (see ch. 4.7). However, already the available dataset can yield more data. Additional structures like synaptic vesicles could be reconstructed and analyzed. Postsynaptic structures of ChAT+ axon contacts could be traced back and categorized to get a more defined view of the targets of ACh.

Moreover, the somatostatin (SST) expressing interneuron class has not been analyzed in this project, although it is known to be involved in the local disinhibitory circuit where ChAT+, VIP+ and PV+ neurons modulate each other and the activity of principal cells (fig. 4). Imaging and reconstructing SST+ cells and their connections with ChAT+ axons will provide a more complete view of the connectivity and mode of action of ACh on cortical inhibitory interneurons.

## 4.9 Conclusion

The aim of this project was to characterize VIP+, PV+ cells and ChAT+ axons and their connections. We found that VIP+ and PV+ cells receive more excitatory than inhibitory input, although the inhibitory input on distal VIP+ dendrites is still substantial, corroborating the importance of cross-talk between inhibitory interneurons in cortical microcircuits.

Additionally, considering the connections made by neuromodulatory axons such as cholinergic axons, it may not be correct to impose strict rules on synapse characterization at the EM level. Despite analysing 333 µm of ChAT+ axons we did not observe clear synaptic connections. However, vesicles were abundant, occasionally in close proximity to membrane contacts with interneurons. Therefore, it would be important

to understand where the ACh receptors are located to fully identify the nature of the specificity of these contacts. The results indicate that a less stringent approach needs to be taken when analysing connections of neuromodulatory axons in EM images. This could be particularly relevant in the light of the significant investments that are being made into mapping neural connections of entire microcircuits to produce complete circuit diagrams of the brain. Refraining from clearly categorizing these contacts into synapse or non-synapses might enable a more neutral view on the mechanisms and functionality of the subtle and delicate communication between modulatory neurons and their targets.

# Bibliography

- Alitto, H. J. and Dan, Y. (2013). Cell-type-specific modulation of neocortical activity by basal forebrain input. *Frontiers in Systems Neuroscience*, 6(January):1–12.
- Arber, C., Houlden, H., Li, A., Patani, R., Wray, S., and Wiethoff, S. (2015). Using human induced pluripotent stem cells to model cerebellar disease: Hope and hype. *Journal of Neurogenetics*, 29(2-3):95–102.
- Bopp, R., Holler-Rickauer, S., Martin, K. A. C., and Schuhknecht, G. F. P. (2017). An Ultrastructural Study of the Thalamic Input to Layer 4 of Primary Motor and Primary Somatosensory Cortex in the Mouse. *The Journal of neuroscience : the official journal of the Society for Neuroscience*, 37(9):2435–2448.
- Boyde, A. and Boyde, S. (1979). Further studies of specimen volume changes during processing for sem : including some plant tissue. *Scanning electron microscopy*, pages 117–124.
- Cauli, B., Tong, X.-K., Rancillac, A., Serluca, N., Lambolez, B., Rossier, J., and Hamel, E. (2004). Cortical GABA interneurons in neurovascular coupling: relays for subcortical vasoactive pathways. *The Journal of neuroscience : the official journal of the Society for Neuroscience*, 24(41):8940–8949.
- Celio, M. R. (1986). Parvalbumin in most gamma-aminobutyric acid-containing neurons of the rat cerebral cortex. *Science*, 231(4741):995 LP – 997.
- Cobos, I., Calcagnotto, M. E., Vilaythong, A. J., Thwin, M. T., Noebels, J. L., Baraban, S. C., and Rubenstein, J. L. R. (2005). Mice lacking Dlx1 show subtype-specific loss of interneurons, reduced inhibition and epilepsy. *Nature neuroscience*, 8(8):1059–1068.
- Crochet, S. and C H Petersen, C. (2006). Correlating whisker behavior with membrane potential in barrel cortex of awake mice. *Nature neuroscience*, 9:608–10.
- David, C., Schleicher, A., Zuschratter, W., and Staiger, J. F. (2007). The innervation of parvalbumin-containing interneurons by VIP-immunopositive interneurons in the primary somatosensory cortex of the adult rat. *The European journal of neuroscience*, 25(8):2329–2340.

---

## Bibliography

- Descarries, L., Gisiger, V., and Steriade, M. (1997). Diffuse transmission by acetylcholine in the cns. *Progress in Neurobiology*, 53(5):603 – 625.
- Descarries, L. and Mechawar, N. (2000). Ultrastructural evidence for diffuse transmission by monoamine and acetylcholine neurons of the central nervous system. 125(September 1989).
- Eggermann, E., Kremer, Y., Crochet, S., and Petersen, C. C. (2014). Cholinergic Signals in Mouse Barrel Cortex during Active Whisker Sensing. *Cell Reports*, 9(5):1654–1661.
- Feldmeyer, D., Brecht, M., Helmchen, F., Petersen, C. C., Poulet, J. F., Staiger, J. F., Luhmann, H. J., and Schwarz, C. (2013). Barrel cortex function. *Progress in Neurobiology*, 103:3–27.
- Fu, Y., Kaneko, M., Tang, Y., Alvarez-Buylla, A., and Stryker, M. P. (2015). A cortical disinhibitory circuit for enhancing adult plasticity. *eLife*, 4:e05558.
- Fu, Y., Tucciarone, J. M., Espinosa, J. S., Sheng, N., Darcy, D. P., Nicoll, R. A., Huang, Z. J., and Stryker, M. P. (2014). A cortical circuit for gain control by behavioral state. *Cell*, 156(6):1139–1152.
- Geiger, J. R., Melcher, T., Koh, D. S., Sakmann, B., Seburg, P. H., Jonas, P., and Monyer, H. (1995). Relative abundance of subunit mRNAs determines gating and Ca 2+ permeability of AMPA receptors in principal neurons and interneurons in rat CNS. *Neuron*, 15(1):193–204.
- Gonchar, Y., Wang, Q., and Burkhalter, A. (2008). Multiple distinct subtypes of GABAergic neurons in mouse visual cortex identified by triple immunostaining. 1(March).
- Haeusser, M., Spruston, N., and Stuart, G. J. (2000). Diversity and dynamics of dendritic signaling. *Science (New York, N.Y.)*, 290(5492):739–744.
- Hu, H., Gan, J., and Jonas, P. (2014). Fast-spiking, parvalbumin+ GABAergic interneurons: From cellular design to microcircuit function. *Science*, 345(6196).
- Kawaguchi, Y., Katsumaru, H., Kosaka, T., Heizmann, C. W., and Hama, K. (1987). Fast spiking cells in rat hippocampus (CA1 region) contain the calcium-binding protein parvalbumin. *Brain Research*, 416(2):369–374.
- Knott, G. and Genoud, C. (2013). Is EM dead? *Journal of Cell Science*, 126(20):4545–4552.

---

## Bibliography

- Kuki, T., Fujihara, K., Miwa, H., Tamamaki, N., Yanagawa, Y., and Mushiake, H. (2015). Contribution of parvalbumin and somatostatin-expressing gabaergic neurons to slow oscillations and the balance in beta-gamma oscillations across cortical layers. *Frontiers in Neural Circuits*, 9.
- Lee, S., Kruglikov, I., Huang, Z. J., Fishell, G., and Rudy, B. (2013). A disinhibitory circuit mediates motor integration in the somatosensory cortex. *Nature Neuroscience*, 16(11):1662–1670.
- Letzkus, J. J., Wolff, S. B. E., Meyer, E. M. M., Tovote, P., Courtin, J., Herry, C., and Lüthi, A. (2011). A disinhibitory microcircuit for associative fear learning in the auditory cortex. *Nature*, 480:331.
- Levinson, A. J., Young, L. T., Fitzgerald, P. B., and Daskalakis, Z. J. (2007). Cortical Inhibitory Dysfunction in Bipolar Disorder: A Study Using Transcranial Magnetic Stimulation. *Journal of Clinical Psychopharmacology*, 27(5).
- Li, L. Y., Xiong, X. R., Ibrahim, L. A., Yuan, W., Tao, H. W., and Zhang, L. I. (2015). Differential Receptive Field Properties of Parvalbumin and Somatostatin Inhibitory Neurons in Mouse Auditory Cortex. *Cerebral Cortex*.
- Lodato, S., Arlotta, P., and Biology, R. (2016). HHS Public Access. pages 699–720.
- Lui, J., Hansen, D., and Kriegstein, A. (2011). Development and Evolution of the Human Neocortex. *Cell*, 146(1):18–36.
- MacLachlan, C., Sahlender, D. A., Hayashi, S., Molnár, Z., and Knott, G. (2018). Block Face Scanning Electron Microscopy of Fluorescently Labeled Axons Without Using Near Infra-Red Branding. 12(November):1–8.
- Magistretti, P. J. and Pellerin, L. (1999). Cellular mechanisms of brain energy metabolism and their relevance to functional brain imaging. *Philosophical transactions of the Royal Society of London. Series B, Biological sciences*, 354(1387):1155–1163.
- Malenka, R. C. (1991). Postsynaptic Factors Control the Duration of Synaptic Enhancement in Area CA1 of the Hippocampus. 6:53–60.
- Markram, H., Toledo-Rodriguez, M., Wang, Y., Gupta, A., Silberberg, G., and Wu, C. (2004). Interneurons of the neocortical inhibitory system. *Nature Reviews Neuroscience*, 5(10):793–807.

---

## Bibliography

- Munoz, W., Tremblay, R., Levenstein, D., and Rudy, B. (2017). Layer-specific modulation of neocortical dendritic inhibition during active wakefulness. *Science (New York, N.Y.)*, 355(6328):954–959.
- Palay, S. L., Sotelo, C., Peters, A., and Orkand, P. M. (1968). THE AXON HILLOCK AND THE INITIAL SEGMENT. (17).
- Petersen, C. C. and Crochet, S. (2013). Synaptic Computation and Sensory Processing in Neocortical Layer 2/3. *Neuron*, 78(1):28–48.
- Pfeffer, C. K. (2014). Inhibitory neurons: Vip cells hit the brake on inhibition. *Current Biology*, 24(1):R18–R20.
- Pfeffer, C. K., Xue, M., He, M., Huang, Z. J., and Scanziani, M. (2013). Inhibition of inhibition in visual cortex: The logic of connections between molecularly distinct interneurons. *Nature Neuroscience*, 16(8):1068–1076.
- Pi, H.-J., Hangya, B., Kvitsiani, D., Sanders, J. I., Huang, Z. J., and Kepecs, A. (2013). Cortical interneurons that specialize in disinhibitory control. *Nature*, 503:521.
- Picciotto, M. R., Higley, M. J., and Mineur, Y. S. (2012). NIH Public Access. *Neuron*, 76(1):116–129.
- Pinto, L., Goard, M. J., Estandian, D., Xu, M., Kwan, A. C., Lee, S. H., Harrison, T. C., Feng, G., and Dan, Y. (2013). Fast modulation of visual perception by basal forebrain cholinergic neurons. *Nature Neuroscience*, 16(12):1857–1863.
- Proenneke, A., Scheuer, B., Wagener, R. J., Möck, M., Witte, M., and Staiger, J. F. (2015). Characterizing VIP neurons in the barrel cortex of VIPcre/tdTomato mice reveals layer-specific differences. *Cerebral Cortex*, 25(12):4854–4868.
- Rogasch, N. C., Daskalakis, Z. J., and Fitzgerald, P. B. (2014). Cortical inhibition, excitation, and connectivity in schizophrenia: a review of insights from transcranial magnetic stimulation. *Schizophrenia bulletin*, 40(3):685–696.
- Rudy, B., Fishell, G., Lee, S., and Hjerling-Leffler, J. (2011). Three groups of interneurons account for nearly 100% of neocortical GABAergic neurons. *Developmental neurobiology*, 71(1):45–61.
- Sarter, M., Parikh, V., and Howe, W. M. (2009). Sarter et al 2009 Phasic Ach release and vol trans. 10(may):383–390.

---

## Bibliography

- Staiger, J. F., Masanneck, C., Schleicher, A., and Zuschratter, W. (2004). Calbindin-containing interneurons are a target for VIP-immunoreactive synapses in rat primary somatosensory cortex. *The Journal of comparative neurology*, 468(2):179–189.
- Staiger, J. F., Moeck, M., Proenneke, A., and Witte, M. (2015). What types of neocortical gabaergic neurons do really exist? *e-Neuroforum*, 6(2):49–56.
- Taniguchi (2012). NIH Public Access. *Changes*, 29(6):997–1003.
- Thiele, A. (2013). Muscarinic Signaling in the Brain. *Annual Review of Neuroscience*, 36(1):271–294.
- Tremblay, R., Lee, S., and Rudy, B. (2017). Properties To Circuits. 91(2):260–292.
- Turrini, P., Casu, M., Wong, T., Koninck, Y. D., da Silva, A. R., and Cuello, A. (2001). Cholinergic nerve terminals establish classical synapses in the rat cerebral cortex: synaptic pattern and age-related atrophy. *Neuroscience*, 105(2):277 – 285.
- Wanaverbecq, N., Semyanov, A., Pavlov, I., Walker, M. C., and Kullmann, D. M. (2007). Cholinergic axons modulate gabaergic signaling among hippocampal interneurons via post-synaptic a7 nicotinic receptors. *Journal of Neuroscience*, 27(21):5683–5693.
- Wang, X. J. and Yang, G. R. (2018). A disinhibitory circuit motif and flexible information routing in the brain. *Current Opinion in Neurobiology*, 49:75–83.
- Wang, Y., Balaji, V., Kaniyappan, S., Krüger, L., Irsen, S., Tepper, K., Chandupatla, R., Maetzler, W., Schneider, A., Mandelkow, E., and Mandelkow, E.-M. (2017). The release and trans-synaptic transmission of Tau via exosomes. *Molecular Neurodegeneration*, 12(1):5.
- Wittmann, M., Queisser, G., Eder, A., Wiegert, J. S., Bengtson, C. P., Hellwig, A., Wittum, G., and Bading, H. (2009). Synaptic Activity Induces Dramatic Changes in the Geometry of the Cell Nucleus : Interplay between Nuclear Structure , Histone H3 Phosphorylation , and Nuclear Calcium Signaling. 29(47):14687–14700.
- Wollner, D. A. and Catterall, W. A. (1986). Localization of sodium channels in axon hillocks and initial segments of retinal ganglion cells. 83(November):8424–8428.
- Zhang, S., Xu, M., Kamigaki, T., Hoang Do, J. P., Chang, W.-C., Jenvay, S., Miyamichi, K., Luo, L., and Dan, Y. (2014). Long-range and local circuits for top-down modulation of visual cortex processing. *Science*, 345(6197):660–665.

Zhao, S., Ting, J. T., Atallah, H. E., Qiu, L., Tan, J., Gloss, B., Augustine, G. J., Deisseroth, K., Luo, M., Graybiel, A. M., and Feng, G. (2011). Cell type-specific channelrhodopsin-2 transgenic mice for optogenetic dissection of neural circuitry function. *Nature Methods*, 8(9):745–755.

# Acknowledgements

I would like to thank Dr. Graham Knott and Prof. Carl Petersen for their supervision. Moreover, I would like to thank Dr. Knott for performing the mice perfusions, Stephanie Rosset for staining and embedding the brain slices, Anaelle Dubois for assisting me with the SBEM imaging, and Jérôme Durochet for helping with the EM image processing and 3D modeling. Moreover, I would like to thank the Neurasmus for this amazing mobility scheme which allowed me to get to see very various scientific set up, and FENS for financing part of my project at EPFL. Finally, I would like to thank my family, my Nelo and my second family in Germany for helping me through the stressful times.

# **Declaration of independent work**

Herewith I declare, that I prepared the Master's Thesis "BLABLABLA" on my own and with no other sources and aids than quoted.

Göttingen, \_\_\_\_\_ Signature: \_\_\_\_\_